JGR Atmospheres

RESEARCH ARTICLE
10.1029/2023JD039043

Summertime Airborne Measurements of Ammonia Emissions From Cattle Feedlots and Dairies in Northeastern Colorado

Julieta F. Juncosa Calahorrano[1], Ilana B. Pollack[1], Amy P. Sullivan[1], J. Robert Roscioli[2], Dana R. Caulton[3], Megan E. McCabe[3], En Li[1], Jeffrey R. Pierce[1], and Emily V. Fischer[1]

[1]Department of Atmospheric Science, Colorado State University, Fort Collins, CO, USA, [2]Aerodyne Research Inc., Billerica, MA, USA, [3]Department of Atmospheric Science, University of Wyoming, Laramie, WY, USA

Key Points:

- We report ammonia emission rates and emission ratios with respect to methane for beef cattle feedlots and dairies in Colorado
- The NH_3 EmR estimates are generally larger than prior estimates. NH_3 EmR estimates for feedlots are four times larger than those for dairies
- NH_3 inferred emission rates for cattle feedlots range from 4 to 29 g $NH_3 \cdot h^{-1} \cdot hd^{-1}$ for sampling temperatures between 19 and 27°C

Supporting Information:

Supporting Information may be found in the online version of this article.

Correspondence to:

J. F. Juncosa Calahorrano,
jjuncosa@colostate.edu

Citation:

Juncosa Calahorrano, J. F., Pollack, I. B., Sullivan, A. P., Roscioli, J. R., Caulton, D. R., McCabe, M. E., et al. (2023). Summertime airborne measurements of ammonia emissions from cattle feedlots and dairies in northeastern Colorado. *Journal of Geophysical Research: Atmospheres*, *128*, e2023JD039043. https://doi.org/10.1029/2023JD039043

Received 13 APR 2023
Accepted 12 OCT 2023

Abstract Phase One of the Transportation and Transformation of Ammonia (TRANS^{2}Am) field campaign took place in northeastern Colorado during the summer of 2021. One of the goals of TRANS^{2}Am was to measure ammonia (NH_3) emissions from cattle feedlots and dairies. Most of these animal husbandry facilities are co-located within oil and gas development, an important source of methane (CH_4) and ethane (C_2H_6) in the region. Phase One of TRANS^{2}Am included 12 near-source research flights. We present estimates of NH_3 emissions ratios with respect to CH_4 (NH_3 EmR), with and without correction of CH_4 from oil and gas, for 29 feedlots and dairies in the region. The data shows larger emissions ratios than previously reported in the literature with a large range of values (i.e., 0.1–2.6 ppbv ppbv^{-1}). Facilities housing cattle and dairy had a mean (std) of 1.20 (0.63) and 0.29 (0.08) ppbv ppbv^{-1}, respectively. We also found that only 15% of the total ammonia (NH_x) is in the particle phase (i.e., NH_4^+) near major sources during the warm summertime months. We examined the evolution of NH_3 in one plume that was sampled at different distances and altitudes up to 25 km downwind and estimated the NH_3 lifetime against deposition and partitioning to the particle phase to be 87–120 min. Finally, we calculated estimates of NH_3 emission rates from four optimally sampled facilities. These ranged from 4 to 29 g $NH_3 \cdot h^{-1} \cdot hd^{-1}$.

Plain Language Summary Animal husbandry operations are significant emitters of gases that impact climate change and the health of humans and ecosystems. Northeastern Colorado has a large number of animal husbandry facilities. Many of these facilities are located nearby oil and gas operations, which emit some of the same gases as animal husbandry facilities. During the summer of 2021, as part of the Transportation and Transformation of Ammonia field camping, we deployed instruments to measure methane, ammonia, ethane, and water-soluble aerosol components in northeastern Colorado using the University of Wyoming King Air research aircraft. In this manuscript, we quantify ammonia emissions from 29 animal husbandry facilities and study their relationship with ambient temperature, relative humidity, time of day, and distance from the facility.

1. Introduction

Ammonia (NH_3) is the most important base in the atmosphere. It is a precursor for the formation of fine particulate matter ($PM_{2.5}$) (Bauer et al., 2016), which impacts human health and Earth's radiative balance. It also is a major determinant of aerosol pH, with implications for cloud formation and aerosol chemistry (Karydis et al., 2021). NH_3 can also readily undergo dry and wet deposition, altering the natural nitrogen (N) cycle. Excess N can cause soil acidification (Bobbink et al., 2010) and eutrophication of water bodies (Zhan et al., 2017).

Globally, large sources of NH_3 include agriculture, biomass burning, industrial activities, and combustion (Meng et al., 2017; Xu et al., 2019). Agriculture activities, including livestock and fertilizer application, account for over 80% of NH_3 emissions in the United States, Europe, and China (Van Damme et al., 2018). It is estimated that NH_3 from agriculture can contribute to 15%–50% of the $PM_{2.5}$ in these countries (Wyer et al., 2022). The deposition of N in the United States has recently switched from being dominated by oxidized N to being dominated by reduced N (e.g., NH_3) (Li et al., 2016). This is partly due to successful regulatory measures to decrease the emission of nitrogen oxides (i.e., NO_x) accompanied by unregulated and increasing emissions of NH_3 (Davidson et al., 2011; Kim et al., 2006; Tong et al., 2015). Because they are unregulated and have historically been difficult to measure, United States NH_3 emissions are uncertain and have large errors in national emissions inventories (Heald et al., 2012). Therefore, careful characterization of NH_3 emissions is important for improving air quality and human and ecosystem health and to better understand the impact of aerosols on climate.

Most of the NH_3 emissions in the United States are attributed to fertilizer application (21%) and livestock (59%) (Environmental Protection Agency (EPA), The National Emission Inventory (NEI), 2017). The United States is the largest producer of beef in the world and 80% of the country's beef cattle and dairy cows are concentrated in the Great Plains region and in parts of the Corn Belt, Southwest, and Pacific Northwest (USDA, 2012). NH_3 from livestock is emitted to the atmosphere through biological and chemical bacterial decomposition of excreted N. Livestock eat protein- and N-rich feed to yield desirable N-rich products (i.e., meat, milk, and eggs). However, most of the N in the feed (70%–95%) is eliminated through excretion rather than converted to the N-rich products, resulting in large emissions of NH_3 and other N compounds (i.e., nitrous oxide [N_2O]) (Huntington & Archibeque, 2000). Other gasses emitted from animal feeding operations include three greenhouse gasses: methane (CH_4), N_2O, and carbon dioxide (CO_2). CH_4 and N_2O have 28 and 265 times the 100-year Global Potential Warming of CO_2, respectively (IPCC, 2021). Livestock emits CH_4 through enteric fermentation. Emitted NH_3 and CH_4 from livestock vary greatly depending on diurnal and seasonal cycles and the number of animals in each facility. Eventually, NH_3 emitted into the atmosphere will deposit to the water or soil surfaces as gas or particles or through precipitation events. Although, as mentioned above, NH_3 deposition could negatively affect ecosystems such as water eutrophication and soil acidification, in N-poor ecosystems such as N-starved farmlands adjacent to CAFOs, NH_3 deposition could have beneficial fertilization effects (Preece et al., 2017). Manure treatment and storage methods greatly influence the emissions of NH_3 and CH_4 (Eilerman et al., 2016). Proposed strategies to reduce the emission of NH_3 to the environment include reducing high protein feed, frequent removal of manure and separation of it from urine, filtration of emissions from confinement facilities (i.e., scrubbers/filters), controlling conditions to keep low temperatures and low pH in the manure, and injection or incorporation of NH_3 into the soil soon after fertilizer application (Ndegwa et al., 2008).

Historical challenges in measuring NH_3 (i.e., Miller et al., 2014; Roscioli et al., 2016) have limited progress on emissions estimates for this pollutant. Recent advances in measuring NH_3, including in-situ measurements (e.g., Ellis et al., 2010; Pollack et al., 2019; Roscioli et al., 2016) and satellite retrievals (e.g., Cady-Pereira et al., 2023; Van Damme et al., 2018), have increased our awareness of the importance of measuring NH_3 from large point sources. The availability of new observations has helped models to represent NH_3 emissions in the United States (Zhu et al., 2015) and worldwide (Clarisse et al., 2009) better and shine light on the potential underestimation of emission inventories on NH_3 emissions (e.g., Heald et al., 2012; Nowak et al., 2012). Considerable deposition of N in and around sensitive ecosystems has been identified as one of the leading problems of NH_3 emission in the United States (Benedict et al., 2013a, 2013b) and globally (Liu et al., 2022). Due to the large number of NH_3 emission sources and the uncertainty in the magnitude of their NH_3 emission, more detailed measurements are needed.

Here, we report on summertime airborne observations of NH_3 and CH_4 collected over northeastern Colorado during Phase One of the Transportation and Transformation of Ammonia ($TRANS^2Am$) field intensive. We use these data to produce (a) a summary of summertime NH_3 emission ratios with respect to CH_4 representing 29 beef cattle and dairy facilities and their dependence on temperature and time of day, (b) estimates of the differences between emission ratios associated with beef cattle and dairy cows facilities, and (c) NH_3 emission rate estimates as a function of maximum animal capacity for select comprehensively sampled facilities.

2. Methods

2.1. Study Region

Colorado has a large number of livestock operations (Figure 1a), and the majority and largest facilities (in terms of maximum reported animal capacity) in this region house beef cattle and dairy cows (blue and pink dots, respectively, in Figure 1). Over 1 million animals are clustered in counties in the northeast part of the state (i.e., Larimer, Weld, Morgan, Washington, Yuma, Logan, and Phillips). While many of these operations are large sources of trace gases, separating and quantifying the emissions from individual facilities is difficult because many facilities are located in close proximity to the dense oil and gas development throughout much of the area (i.e., Denver-Julesburg basin—black dots in Figures 1a and 1b), as well as large urban centers (i.e., vehicle traffic and industrial sources along the Colorado Front Range corridor). Rocky Mountain National Park (RMNP) and other sensitive high-alpine areas are located directly west of the polluted Colorado Front Range. N deposition in this area is dominated by reduced N during upslope events (easterly winds) that carry emissions from the eastern plains to the mountain ecosystems (Benedict et al., 2013a, 2013b; Li et al., 2016; Pan et al., 2021). Agricultural

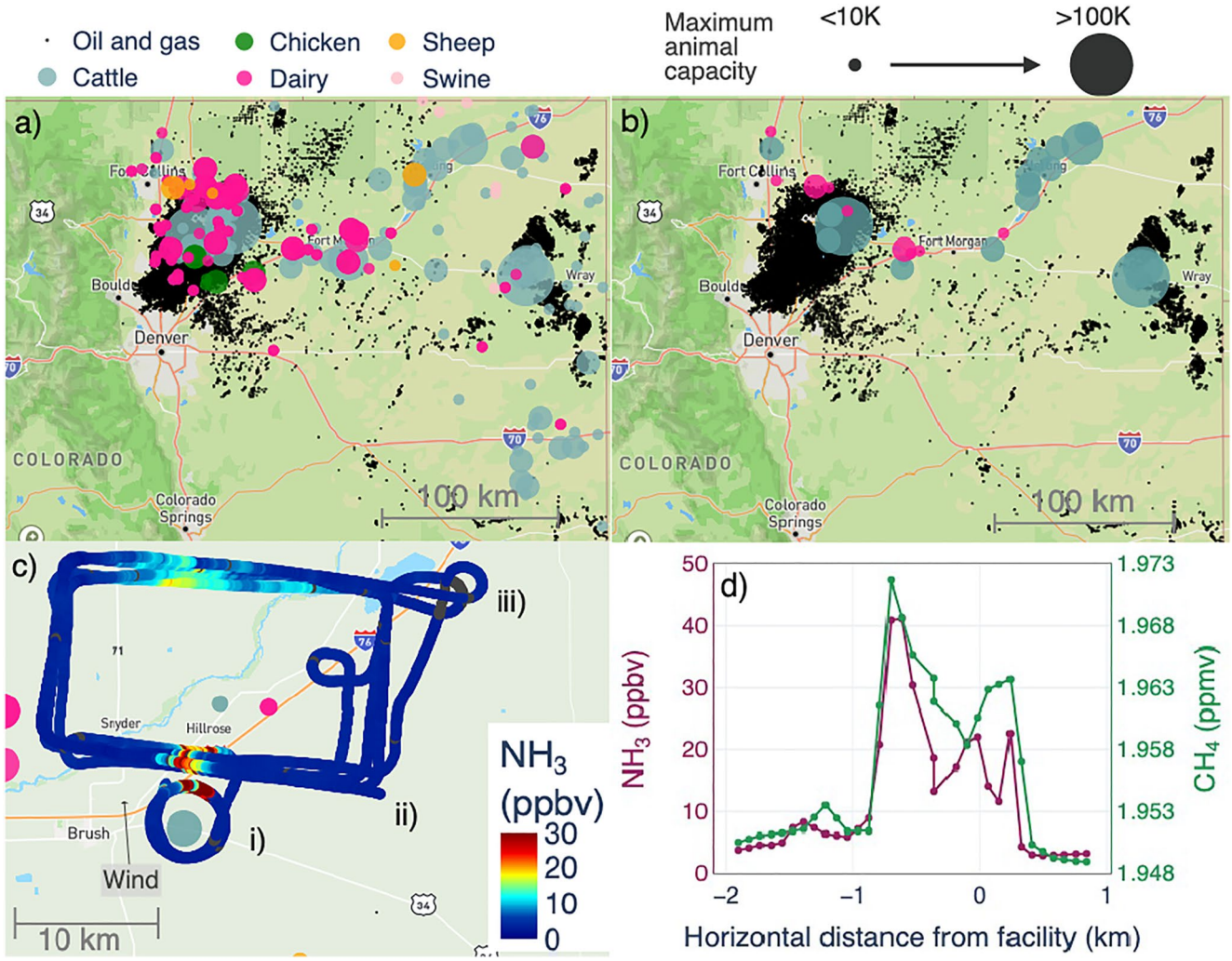

Figure 1. (a) Map of northeastern Colorado showing the large number of livestock facilities in the region. The different colors signify the type of animal housed at each facility, and the size of the marker is proportional to the maximum animal capacity. Black dots indicate the locations of active oil and gas wells as of 2015. (b) Same map as (a) but only including facilities sampled systematically during Phase One of TRANS^{2}Am. (c) Flight track of the UWKA colored by NH_3 (ppbv) during the sampling of Facility 1 (F01; refer to Table 1 for more information) on 2 August 2021. This example flight track is representative of the general sampling strategy used during TRANS^{2}Am. Letters (i, ii, iii) refer to different vertical transects used for emission rate calculations (refer to Figure 6 and Section 2.5.5 for more information). (d) Example of a transect with colocated enhancements of NH_3 (ppbv; purple) and CH_4 (ppmv; green) versus horizontal distance from the facility. Note that we include non-plume background values in each transect (i.e., tails on each side of each transect).

emissions traveling due west cross over urban centers where other urban pollutants (i.e., nitric acid [HNO_3]) are available for forming fine particulate matter ($PM_{2.5}$) through ammonium nitrate (NH_4NO_3) formation.

Several recent measurement campaigns have aimed at characterizing emissions from animal husbandry in the region. For example, Eilerman et al. (2016) reported on a year-long ground-based survey of four facilities housing beef, dairy, and sheep, and this report summarizes their diurnal and seasonal variations. The study highlights the strong relationship between NH_3 emissions and time of the day. Kille et al. (2019) apportioned CH_4 emissions in the region to either oil and gas or agriculture using ethane (C_2H_6) and NH_3 as tracers for each of these sources, respectively. This resulted in NH_3 emissions ratios with respect to CH_4 for the region. The Ammonia Phase Partitioning and Transport (APART) field campaign was the proof of concept field study leading to TRANS^{2}Am. They characterized plumes downwind of five beef cattle facilities during November 2019, showing that NH_3 near-source emissions can be tracked using airborne platforms. They found that large NH_3 emissions ratios can be observed during cooler temperature conditions in the region (McCabe et al., 2023; Pollack, McCabe, et al., 2022). Finally, Golston et al. (2020) deployed three mobile platforms in the summer of 2014. They intercepted NH_3 and CH_4 plumes downwind of 43 facilities (15 beef, 25 dairy, 1 sheep, and 2 poultry) in the region

Table 1
Summary of Facility Information, Meteorological Conditions, NH_3 EmR, and Emission Rates for Beef Cattle [C] and Dairy [D] Facilities Sampled During Phase One of TRANS²Am

Facility name and flight number [animal type] C = cattle D = dairy	Lat (°)	Lon (°)	Animal Max. capacity	T (°C)	RH (%)	Mean NH_3 EmR [std] (ppbv ppbv^{-1})	Emission rates [mean] (gNH_3 · h^{-1} · hd^{-1})
F01_RF01 [C]	40.26203	−103.5426	42,000	23	30	1.7 [0.5]	10, 16, 26 [17.3]
F01_RF09 [C]	40.26203	−103.5426	42,000	25	45	1.0 [0.1]	No
F02_RF02 [D]	40.56931	−104.61205	9,742	19	54	0.5 [0.1]	No
F03_RF02 [D]	40.57394	−104.69556	13,150	19	54	0.4 [0.03]	No
F04_RF03 [C]	40.37826	−104.5098	100,100	25	27	0.9 [0.2]	No
F04_RF13 [C]	40.37826	−104.5098	100,100	27	32	1.2 [0.2]	18, 7.5, 29, 10, 16, 8.5, 4 [11.8]
F05_RF03 [C]	40.30662	−104.6082	15,000	26	27	0.2 [0.1]	No
F06_RF03 [D]	40.44983	−104.4851	13,384	27	24	0.2 [0.1]	No
F07_RF05 [D]	40.60447	−104.9498	4,235	28	23	0.2 [0.1]	No
F08_RF05 [C]	40.75772	−104.976	25,024	27	19	0.3 [0.2]	No
F09_RF05 [D]	40.83852	−104.9778	7,500	27	17	0.5 [0.2]	No
F10_RF06 [C]	40.5125	−103.3255	30,024	24	25	1.3 [0.3]	No
F11_RF09 [C]	40.5125	−103.3255	30,024	30	32	1.7 [0.1]	No
F12_RF06 [C]	40.5795	−103.3087	30,000	25	28	1.7 [0.2]	No
F13_RF06 [C]	40.7611	−103.1271	10,500	23	33	0.5 [0.6]	No
F13_RF14 [C]	40.7611	−103.1271	10,500	30	16	1.5 [0.3]	No
F14_RF06 [C]	40.78102	−102.9658	65,100	23	35	1.4 [0.03]	No
F14_RF14 [C]	40.78102	−102.9658	65,100	31	20	2.2 [0.5]	No
F15_RF06 [C]	40.83167	−102.933	20,012	23	36	1.1 [0.2]	No
F15_RF14 [C]	40.83167	−102.933	20,012	30	22	2.1 [1.0]	No
F16_RF06 [C]	40.66031	−103.1701	22,030	25	32	1.1 [0.04]	No
F16_RF14 [C]	40.66031	−103.1701	22,030	28	24	1.2 [0.3]	No
F17_RF06 [C]	40.7064	−103.2484	10,000	25	28	2.6 [0.5]	No
F18_RF06 [C]	40.6323	−103.3159	28,000	25	27	0.6 [0.1]	No
F19_RF08 [C]	40.16511	−104.132	35,000	19	93	1.2 [0.3]	13, 6, 10 [9.6)]
F20_RF09 [D]	40.336	−103.4747	17,000	25	44	0.3 [0.1]	No
F21_RF09 [C]	40.5798	−103.3091	30,000	29	35	2.1 [0.1]	No
F22_RF09 [C]	40.5905	−103.3063	NA	29	33	1.5 [0.3]	No
F23_RF08 [C]	40.20565	−104.1123	9,510	17	83	0.1 [0.04]	No
F24_RF08 [D]	40.26543	−104.1233	14,066	18	77	0.3 [0.1]	No
F25_RF08 [C&D]	40.2439	−104.0744	NA	19	77	0.3 [0.03]	No
F26_RF08 [D]	40.2409	−104.0002	NA	17	81	0.3 [0.03]	No
F27_RF11 [C]	40.11569	−102.5851	125,150	26	35	1.4 [0.2]	16, 17, 15.5, 21, 15.5 [17]
F28_RF11 [C]	40.1779	−102.5675	54,060	27	35	1.5 [0.2]	16, 17, 15.5, 21, 15.5 [17]
F29_RF13 [C]	40.43781	−104.6004	34,020	25	41	0.2 [0.1]	No

and found a large underestimation in emissions inventories (i.e., NEI and EDGAR) for NH_3 and CH_4 as well as significant site-to-site variability for NH_3 and CH_4 emissions. The NH_3 emission ratios with respect to CH_4 from all the studies listed above range between 0.17 and 2.7 ppbv ppbv^{-1}. Even fewer studies (Golston et al., 2020; Kille et al., 2017; McCabe et al., 2023) report emission rates of NH_3 (rather than emissions ratios that are normal-

ized by CH_4) in the region. The few studies reporting emission rates of NH_3 highlight the need for more systematic measurements to estimate this magnitude in the region (Golston et al., 2020; Kille et al., 2017; McCabe et al., 2023). Because of the large number of facilities in the region and the large variability in their near-source emissions and evolution, large uncertainties remain on what NH_3 emissions from livestock are in Colorado.

2.2. Campaign Overview

The TRANS^{2}Am field campaign occurred over two phases: (a) 27 July 2021 to 23 August 2021 and (b) 16 August 2022 to 2 September 2022. The field campaign was halted abruptly in August 2021 when the plane was damaged by a collision with a bird and then resumed in 2022. Here, we focus on data collected in 2021. During both phases of TRANS^{2}Am, the University of Wyoming King Air (UWKA) was based at Laramie Regional Airport (KLAR) in Laramie, WY, and was deployed to the northern Colorado Front Range. Figure 1a shows the study region, and Figure 1b shows the facilities for which we provide NH_3 emission estimates. The flight patterns associated with TRANS^{2}Am were designed to meet two sets of objectives. The first set of objectives focuses on near-source emissions and evolution, and the second set of objectives focuses on the regional transport of reduced N into the nearby Rocky Mountains. This manuscript focuses on the first set of objectives. Figure S1 in Supporting Information S1 shows the UWKA flight tracks for the 12 flights targeting near-source emissions. The payload included instrumentation for the measurement of NH_3, HNO_3, C_2H_6, CH_4, carbon monoxide (CO), CO_2, water (H_2O), and water-soluble aerosol components, including ammonium (NH_4^+) and nitrate (NO_3^-). The following sections provide details on the instrumentation and flight patterns deployed during TRANS^{2}Am.

2.3. Airborne Payload

2.3.1. Gas-Phase NH_3

NH_3 was measured using a Colorado State University (CSU) owned and operated commercial (Aerodyne Research, Inc.), single-channel, quantum-cascade tunable infrared laser direct absorption spectrometer (QC-TILDAS) operating at 967 cm^{-1} with and effective path length of 76 m (Ellis et al., 2010; McManus, 2010; McManus et al., 1995; Zahniser et al., 1995). The NH_3 instrument was utilized aboard the UWKA during APART, and details of the instrumentation are available in Pollack, McCabe, et al. (2022). Briefly, the spectrometer uses a direct absorption technique combined with a high sample flow rate (>10 SLPM) to achieve a fast (up to 10 Hz) collection of absolute NH_3 mixing ratios. The NH_3 QC-TILDAS is operated with a heated inertial inlet to provide filter-less separation of particles >300 nm from the sample stream (Ellis et al., 2010). Prior studies show active continuous passivation of the instrument flow path with a strong perfluorinated base improves the time response of the NH_3 QC-TILDAS on mobile platforms (Roscioli et al., 2016). However, we found that a response time of 1–3 s associated with a 90% recovery in NH_3 signal could be maintained during TRANS^{2}Am flights without passive addition by regularly cleaning the instrument sampling surfaces between flights (Pollack et al., 2019). The NH_3 TILDAS is mounted on a vibrationally isolated apparatus and a constant high-frequency vibration is applied to the laser objective to wash out etalon fringe effects due to motion in flight, and thus there is minimal impact of motion sensitivity on instrument precision (Pollack et al., 2019). An injection-style aircraft inlet allows calibration and passivation gases to be introduced into the sample stream within a few centimeters of the inlet tip. The QC-TILDAS was calibrated on the ground between flights via standard addition to the sample stream with a known concentration of NH_3 generated from a temperature-regulated permeation tube. The instrument was regularly zeroed in flight by overflowing the inlet tip with a bottled source of NH_3-free, ultrapure (or "zero") air. The emission rate of the permeation device was calibrated before and after the flight intensive by the NOAA ultraviolet (UV) optical absorption system (Neuman et al., 2003). As reported by Pollack et al. (2019), adding individual uncertainties in quadrature resulted in a combined uncertainty of ±12% of the measured mixing ratio. During TRANS^{2}Am, the 1-Hz NH_3 measured mixing ratio had a 1-Hz precision in flight of 60 pptv corresponding to a 3-sigma detection limit of 180 pptv detection limit. Thus, the overall uncertainty of the instrument is reported as ±12% of the measured mixing ratio plus the 180 pptv detection limit.

2.3.2. Gas-Phase HNO_3

Similar to NH_3, HNO_3 was measured using a commercial (Aerodyne Research, Inc.), single-channel, QC-TILDAS but operating at 1,723 cm^{-1} with an effective path length of 76 m. The HNO_3 instrument is owned by Aerodyne and was operated by CSU during the TRANS^{2}Am field campaign. To make space for the complete payload and to maintain the >10 SLPM sample flow rate for up to 10 Hz collection, the NH_3 and HNO_3 instruments shared

a common aircraft inlet, inertial inlet, and pumping system. Like the NH_3 instrument, the HNO_3 instrument was calibrated on the ground between flights via standard addition to the sample stream with a known concentration of HNO_3 generated from a temperature-regulated permeation device (Kin-Tech; verified by the NOAA UV optical absorption system; Neuman et al., 2003). NH_3 and HNO_3 calibrations were performed individually with copious flushing of the sampling surfaces of the common inlet before the application of the other calibrant. The HNO_3 instrument was regularly "zeroed" with a bottled supply of ultrapure air in flight. Like NH_3, the HNO_3 instrument time response can be improved using active continuous passivation of the sampling surfaces using a strong acid (Roscioli et al., 2016). However, passive addition is not possible when using a combined sample flow path with NH_3. The typical time response of the non-passivated HNO_3 instrument is ∼70 s for a 90% recovery in signal (Roscioli et al., 2016). During TRANS^{2}Am, the time resolution of the HNO_3 instrument was degraded to ∼500 s for 90% signal recovery owing to the use of a common inlet and the HNO_3 QC-TILDAS being positioned downstream of the NH_3 QC-TILDAS in the flow path. Given this long-time response in mind, future comparisons between HNO_3 and other species will require convolution of the fast measurements to the slower HNO_3 data. All the same, HNO_3 data were collected at 10 Hz and averaged to 1 Hz during Phase One of TRANS^{2}Am. The 1-Hz precision was 185 pptv, corresponding to a three-sigma detection limit of 555 pptv at 1 Hz. The HNO_3 spectrometer was also mounted on vibration isolators and a constant high-frequency vibration was applied to the laser objective, and thus motion sensitivity in flight had a minimal impact on precision. The uncertainty related to the 1 Hz samples is ±20% of the measured mixing ratio plus the 555 pptv detection limit.

2.3.3. C_2H_6

C_2H_6 measurements were collected at 1 Hz using a University of Wyoming-owned and operated commercial spectrometer (Aerodyne Research, Inc., Ethane Mini Trace Gas Monitor) employing a similar tunable infrared laser direct absorption spectroscopy (QC-TILDAS) technique as the NH_3 and HNO_3 instruments (Zahniser et al., 1995). The C_2H_6 instrument uses a 2,990 cm^{-1} distributed feedback tunable diode laser, a multipass cell with a path length of 76 m (McManus et al., 1995) and an infrared detector. The C_2H_6 QC-TILDAS is described in detail in Yacovitch et al. (2014). The instrument was zeroed periodically in flight with UZA and calibrated on the ground between flights using a high-accuracy (2.09 ± 0.01 ppb) standard purchased from NOAA ESRL. The 1-Hz precision in flight was 90 ppt resulting in a three-sigma detection limit of 270 ppt.

2.3.4. CH_4, CO, CO_2, and H_2O

CH_4, CO, CO_2, and H_2O were measured simultaneously using a University of Wyoming owned and operated Picarro G2401-m flight-ready analyzer. The instrument samples each species in rotation at ∼0.3 Hz. This closed-path instrument employs infrared cavity ring-down spectroscopy. Ambient air is pumped at a flow rate of 600 mL min^{-1} into an optical cavity that is maintained at 45°C and 140 Torr (Crosson, 2008). Ultra-high reflectivity mirrors allow for multiple passes in the cavity, creating an effective path length of >10 km and leading to high measurement sensitivity (Crosson, 2008). Precision was 30 ppb for CO, 200 ppb for CO_2, and 2 ppb for CH_4 with low drift. The stated low drift for a 24-hr period is 1.5 ppb for CH_4. Most of the flights of TRANS^{2}Am were 4 hr long, which results in <2 ppb of drift (bellow the noise of the instrument). The instrument was zeroed using a bottled supply of UZA and periodically calibrated on the ground between flights with a high-precision NOAA ESRL standard.

2.3.5. Aerosol Composition

Cations, anions, organic acids, and carbohydrates were measured using a Particle-into-Liquid Sampler (PILS) coupled with a fraction collector. This system allows for the collection of liquid samples for offline analysis by ion chromatography. The PILS collects ambient particles into purified water. After particles are grown inside the body of the PILS by mixing the cool airflow with hot steam, the particles are collected by an impactor, and then washed off by a continuous flow of liquid passed over the impactor, providing a liquid sample for analysis (Orsini et al., 2003). The PILS sampled from the NCAR-University of Wyoming Aerosol Inlet mounted to the roof of the King Air (Snider et al., 2018). The PILS size-cut was provided by a non-rotating MOUDI impactor stage with a 50% transmission efficiency at 1 atm ambient pressure of 1 μm (PM1) (Marple et al., 1991). The flow rate for the PILS was 15 LPM pulled off of the main aerosol inlet line. Sodium carbonate and phosphorous acid-coated denuders were placed upstream of the PILS to remove gaseous interferences. A valve upstream of the PILS was manually closed for 10 min, forcing the airflow through a HEPA filter to obtain a measurement of the background in near real-time.

The liquid sample from the PILS was sent to a Brechtel Fraction Collector to collect samples for offline analysis (Sorooshian et al., 2006). The PILS liquid flowrates were set and the fraction collector operated similarly to the

approach used during WE-CAN (Western Wildfire Experiment for Cloud Chemistry, Aerosol Absorption, and Nitrogen) to obtain ∼1.2 mL of liquid sample every 2 min (Sullivan et al., 2022). Pre-loaded carousels were manually switched during flight. After each flight, the vials were unloaded, recapped with solid caps, and transported to CSU in coolers with ice packs to be stored in a 2°C cold room until analyzed.

Each fraction collector vial was brought to room temperature and analyzed for cations, anions, organic acids, and carbohydrates. Only NH_4^+ data is used in the analysis presented here. A Dionex ICS-3000 ion chromatograph was used to measure NH_4^+. A Dionex IonPac CS12A analytical column (3×150 mm^2) employing an eluent of 20 mM methanesulfonic acid at a flow rate of 0.5 mL/min was used. The injection volume was 190 μL with a complete run time of 17 min. Concentrations were blank-corrected using the average of all background samples collected during a specific flight. The limit of detection for NH_4^+ was 0.001 μg/m^3.

2.4. Sampling Approach

2.4.1. Near-Source Sampling Approach

The approach to sample and follow plumes from specific large animal husbandry sources encompassed four steps and an example of this approach is provided in Figure 1c. (a) The UWKA characterized the planetary boundary layer (PBL) after take-off by climbing to the top of the PBL and during descent while approaching the region with the target facility. (b) Once the pilot visually identified the target facility, the UWKA circled it at ∼300 m (∼1,000 ft) agl to identify any obstacles and determine the plume outflow direction. When no obstacles were identified, the UWKA proceeded to perform an additional circle of the facility at ∼150 m (∼500 ft) agl. During these maneuvers, the aircraft remained ∼1 km from the edge of each facility to limit the noise exposure for the animals. (c) Once the plume outflow location was determined, the UWKA completed a set of stacked boxes downwind at different vertical levels. Vertical altitudes were determined to optimize time and sampling throughout the PBL. The vertical distance between flight legs was ∼150 m (∼500 ft). The closest and furthermost legs of the boxes were located ∼5 and 10 km downwind of each facility, respectively. These distances shifted slightly for safety considerations as needed (i.e., air traffic control and obstacles). (d) When plumes were clearly detected 10 km downwind, and time allowed, another set of stack boxes was completed further downwind. Note that this sampling approach was designed to optimize samples of vertical "curtains" used to calculate emission rates rather than following a particular parcel of air downwind from the emission source. The data presented here cannot be considered pseudo-Lagrangian sampling. Figure 1d shows an example transect of NH_3 and CH_4 produced from the sampling approach outlined above. Note the large co-located enhancements in both species (i.e., NH_3 and CH_4).

2.5. Analysis Approach and Calculations

In this study, we use three methods to estimate NH_3 emission ratios relative to CH_4 (NH_3 EmR) for targeted facilities. (a) We determine the average NH_3 normalized excess mixing ratio (NEMR) per horizontal plume transect (Section 2.5.2). (b) We estimate NH_3 EmR from an Ordinary Least Squares (OLS) slope calculated using the observed NH_3 and CH_4 mixing ratios within plume conditions (Section 2.5.3). (c) We determine the NH_3 EmR using the OLS slope that is refined by removing CH_4 mixing ratios associated with emissions from oil and gas operations (Section 2.5.4). All three methods utilize observations identified during transects 10 km or closer to the targeted facility.

2.5.1. Transect Identification

To estimate NH_3 EmR, we identified all plume transects within 10 km downwind of each facility (a total of 232 transects: 156 for cattle facilities and 76 for dairy facilities). The transects are characterized by co-located enhancements with respect to background air for NH_3 and CH_4, as shown in Figure 1d. CH_4 can be considered a conserved tracer because its lifetime against oxidation by the hydroxyl radical (OH), which is its main sink process, is sufficiently long (∼8.3 years) such that it does not undergo any significant loss process in the timescales relevant to this study (i.e., minutes to hours) (Holmes, 2018). Each of our transects includes at least 10 data points of background air or out-of-plume observations on either side of a plume, which is necessary to calculate the enhancement of NH_3 and CH_4 used to calculate the NH_3 NEMR (see Section 2.5.2). Note that in some transects, background mixing ratios differed on each side of a plume.

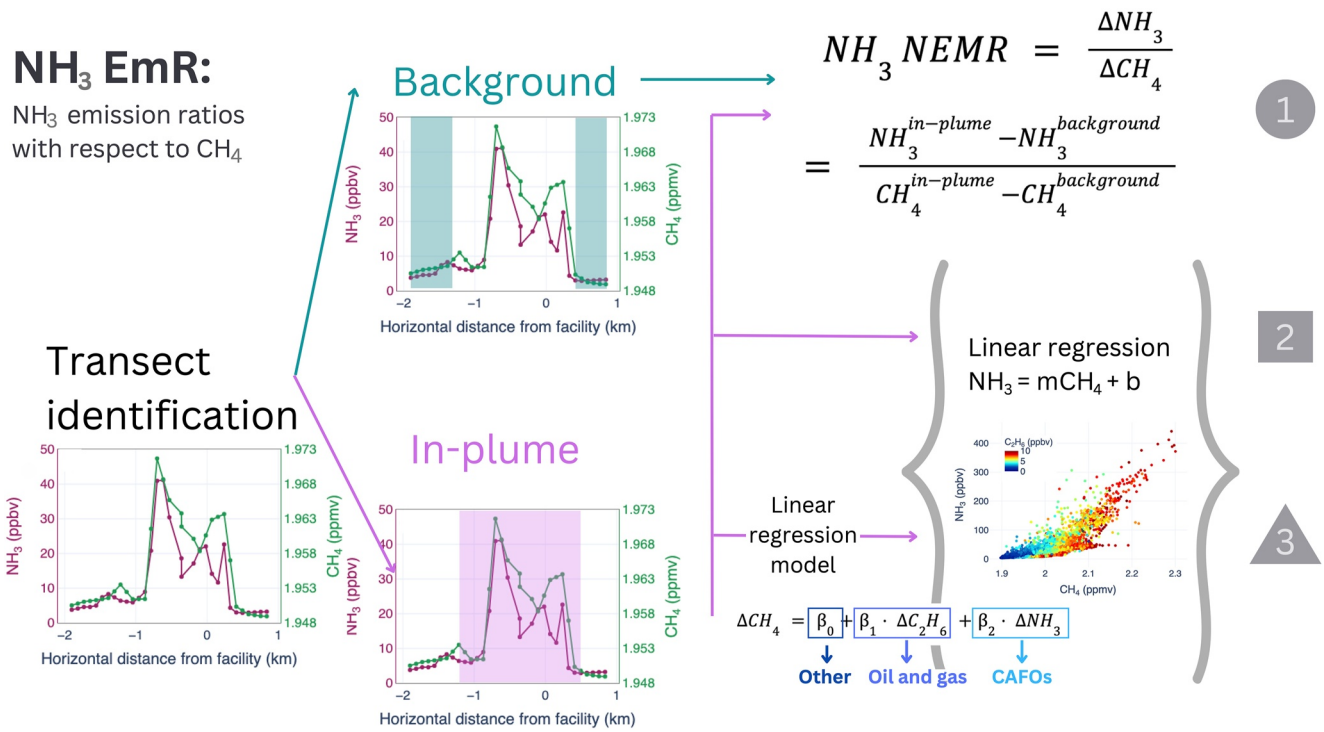

Figure 2. Schematic of the methodology used to calculate the NH_3 emissions ratios with respect to CH_4 (NH_3 EmR) showing the three methods presented in Figure 3.

We calculated the physical age of each intercepted transect downwind of the facility using the distance of the transect downwind from the facility divided by the average wind speed for that transect. We note that most of our intercepted transects fall within the first hour of physical age (see Figure S2 in Supporting Information S1). We also estimated an emission time for each transect by subtracting the physical age for each transect from the average time at which that transect was sampled. A summary of these calculations is presented in Figure S3 in Supporting Information S1. The data collected during TRANS^{2}Am largely represent plumes that have been emitted between mid-morning to early afternoon.

We include transects up to 10 km downwind of a given facility for the NH_3 EmRs calculations described in Sections 2.5.2–2.5.5. Table S1 and Figure S4 in Supporting Information S1 summarize how calculated values vary when they are based on different subsets of the data. Briefly, overall estimates of NH_3 EmRs are slightly higher (2%–7%) when they are based only on transects collected <4 km downwind versus including more data collected further downwind. Next, we describe the three methods used to calculate the NH_3 EmRs, including a detailed explanation of the regression model to isolate oil and gas CH_4 emissions from agricultural CH_4 emissions (Section 2.5.4). Figure 2 shows a schematic of the methods used for the NH_3 EmR calculations.

2.5.2. NH_3 Normalized Excess Mixing Ratios

For each identified transect described above, we calculate the NH_3 NEMR using Equation 1.

$$\mathrm{NH_3\ NEMR} = \frac{\Delta \mathrm{NH_3}}{\Delta \mathrm{CH_4}} = \frac{\overline{\mathrm{NH_3^{in-plume}}} - \overline{\mathrm{NH_3^{background}}}}{\overline{\mathrm{CH_4^{in-plume}}} - \overline{\mathrm{CH_4^{background}}}} \quad (1)$$

In Equation 1, transect-specific in-plume values are defined as the average of 1 Hz observations where NH_3 is > the 25th percentile for that transect. Background values are defined as the average of the observations where NH_3 is ≤ the 25th percentile. Using Equation 1 results in one NEMR value for each transect. A sensitivity analysis using different backgrounds (see Figure S5 in Supporting Information S1) shows that choosing a lower percentile for background values (i.e., fifth percentile) might result in lower plume average values, underestimating the NH_3 EmR by ~5%. Calculating transect-specific NH_3 NEMRs allows us to look at each plume interception independently as a function of time of day, distance from a facility, and vertical location. Note that some of the

analysis in this manuscript uses NH_3 NEMR for individual transects rather than the average NH_3 NEMR within 10 km from the facility (i.e., NH_3 EmR).

2.5.3. OLS Regression

We use the slope calculated from an OSL linear regression of NH_3 versus CH_4 for the observations from all the transects within 10 km as one estimate of the NH_3 EmR. This method uses only in-plume observations. A sensitivity analysis of this method using both background and in-plume observation versus only in-plume observations shows very similar results (Figure S6 in Supporting Information S1).

2.5.4. Linear Regression Analysis With Multiple Predictors to Eliminate Influence of CH_4 From Oil and Gas Sources

Given the close proximity of oil and gas operations to agricultural facilities, we used co-measured C_2H_6 to account for the influence of this potential additional CH_4 source. This is likely a more important issue for correctly interpreting aircraft observations than those collected by vehicles with close access to the perimeter of target facilities; however, Kille et al. (2017) were able to consistently quantify a positive ethane flux out of one of the three dairy sites they sampled using the CU Solar Occultation Flux instrument onboard a mobile vehicle.

Following Kille et al. (2019), we use the *linear model* module from the *sklearn python package* version 1.0.2 to perform a linear regression analysis to the time series of ΔCH_4 (Equation 2) for each facility or group of nearby facilities sampled during each Research Flight (RF) (see Table S2 in Supporting Information S1 for details). This method helps us account for or eliminate the percentage of CH_4 in each observation that is attributed to oil and gas operations in the time series selected for the analysis (Equations 3–5). We use ΔC_2H_6 as the predictor for oil and gas emissions, ΔNH_3 as the predictor for agricultural (i.e., livestock) emissions, and ΔCH_4 as the predictand. This method assumes that oil and gas and livestock operations are the only sources of C_2H_6 and NH_3 in the region, respectively.

$$\Delta CH_4 = \beta_0 + \beta_1 \cdot \Delta C_2H_6 + \beta_2 \cdot \Delta NH_3 \tag{2}$$

The regressions coefficients β_1 and β_2 (ppbv ppbv^{-1}) represent the $\Delta CH_4/\Delta C_2H_6$ and $\Delta CH_4/\Delta NH_3$ ratios, respectively. The coefficient β_0 represents the excess CH_4 above the background that cannot be attributed to any of the two sources. All ΔX (CH_4, C_2H_6, or NH_3) have been calculated using a background, defined as the average of all the data below the 10th percentile of the time series selected for the analysis. We note that using ΔX instead of absolute mixing ratios for each trace gas does not change the values for β_1 and β_2, it only changes the β_0 coefficient, which is related to the regional background selected. Table S2 in Supporting Information S1 shows details for the linear regression analysis, including the regression score, the regression coefficients, and the facilities name and RF that are included in the analysis. We only used model outputs with regression scores (R^2) above 0.4. Once β_0, β_1, and β_2 have been defined from the linear regression model, we use them to calculate the percentage contribution from each emission source (β_0 = other/unexplained CH_4 above regional background, β_1 = CH_4 from oil and gas, and β_2 = CH_4 for agricultural emissions) for each 1-Hz CH_4 observation using Equations 3–5. An example of the percentage contribution from each emission source to CH_4 is shown in Figure S7 in Supporting Information S1 for the same transect shown in Figure 1d.

$$\%\text{Other} = \frac{\beta_0}{\beta_0 + \beta_1 \Delta C_2H_6 + \beta_2 \Delta NH_3} \times 100\% \tag{3}$$

$$\%\text{O\&G} = \frac{\beta_1 \Delta C_2H_6}{\beta_0 + \beta_1 \Delta C_2H_6 + \beta_2 \Delta NH_3} \times 100\% \tag{4}$$

$$\%\text{Ag} = \frac{\beta_2 \Delta NH_3}{\beta_0 + \beta_1 \Delta C_2H_6 + \beta_2 \Delta NH_3} \times 100\% \tag{5}$$

2.5.5. Emission Rate Calculations

We calculated NH_3 emission rates in grams of NH_3 per hour per head of cattle (g $NH_3 \cdot h^{-1} \cdot hd^{-1}$) for four facilities (F01, F04, F19, and F27/28) sampled under ideal wind conditions (i.e., winds >4 ms^{-1}) with a consistent direction, sampling boxes located perpendicular to the wind direction, and minor influence from other emission sources (i.e., other feedlots or dairies)) following the methods by Hacker et al. (2016). The reference frame of the plumes was rotated using the prevalent wind direction to minimize the crosswind component and maximize the

perpendicular wind component. We used different downwind sections (i.e., curtains) of each plume to get multiple independent emission rate estimates per facility (i.e., Figure 1c shows three transects [i.e., curtains] collected downwind of F01 and Figure 6a shows seven transects collected downwind of F04). The 1-Hz data, including calculated instant fluxes (μg $NH_3 \cdot m^{-2} \cdot s^{-1}$ - instantaneous P, T conditions), were averaged to a 200 × 100 m (horizontal × vertical) grid. We assume that the layer near the surface is the same as the data collected at the lowest sampled layer (e.g., ∼150–300 m AGL) corrected by the average topography in each grid cell. We assume that relevant concentration values at the top of the planetary boundary layer height (PBLh) were 10% of the highest available sampled altitude. The PBLh was calculated using potential temperature, water, and wind vertical profiles during descent while approaching the target facilities, following similar methods detailed in Cazorla and Juncosa (2018). We apply a simple linear interpolation (smooth factor = 1) to complete grids without observations. Finally, we integrated the instant fluxes across the total curtain area to obtain a total emission rate per facility at different distances. The maximum animal capacity per facility is based on a livestock registration and permitting database maintained by the Colorado Department of Public Health and Environment (CDPHE, 2017).

3. Results and Discussion

3.1. Emission Ratios for Cattle Feedlots and Dairies

Figure 3 shows NH_3 EmR for 29 facilities housing (a) beef cattle or (b) dairy cows sampled during Phase One of TRANS^{2}Am. Figure 3 shows that there is a large variability in NH_3 EmR between different facilities. Specifically, beef cattle facilities have NH_3 EmR ranging from 0.1 to 2.6 (average 1.2) ppbv $ppbv^{-1}$ and dairies have lower NH_3 EmR ranging from 0.2 to 0.5 (average 0.3 ppbv $ppbv^{-1}$). There is a significant difference between the average NH_3 EmR associated with beef cattle versus dairy facilities. During this study, the NH_3 EmR associated with dairies was on average, four times less than the NH_3 EmR associated with beef cattle (0.3 vs. 1.2 ppbv $ppbv^{-1}$). This difference has been observed previously (Eilerman et al., 2016). Factors that contribute to this pattern include differences in production (milk vs. beef), feeding products, and differences in CH_4 emissions between beef cattle and dairy (Golston et al., 2020). In this data set, dairy NH_3 EmRs are less variable, but this could also be explained by the fewer observations. Note that the different methods used to calculate NH_3 EmR provide similar results with few exceptions. In general, those methods used to correct CH_4 emissions from other sources (i.e., NH_3 NEMR and OLS regression corrected for CH_4) produce similar values, but those values are higher than values produced using methods that do not correct for CH_4 emissions from other sources (OLS regression without correcting for CH_4) (see Figures S4 and S6 in Supporting Information S1). Differences in NH_3 EmR from facilities housing beef cattle versus dairy cows could result from higher emissions of NH_3 from facilities housing beef cattle and/or lower CH_4 emissions from facilities housing dairy cows. A *t*-test of the distribution of NH_3 and CH_4 for facilities housing beef cattle and dairy cows shows that in this data set, both are true (see Figures S8 and S9 in Supporting Information S1). Facilities housing beef cattle have higher mean NH_3 mixing ratios (25.4 vs. 12.3 ppbv) and lower CH_4 mixing ratios (1.978 vs. 1.984 ppmv) compared to dairies.

Table 2 compares our observed NH_3 EmR (and fluxes see Section 3.4) observed in our study to prior observations in the Colorado Front Range. There are several key points from this comparison. (a) Our calculated NH_3 EmR are higher than both Eilerman et al. (2016) and Golston et al. (2020) for both cattle and dairy facilities. This is only partially explained by the time of day of our sampling. The vast majority of the sampling occurred between 10 a.m. and 3 p.m. LT when the diurnal profile of NH_3 EmR typically peaks (see Eilerman et al. (2016), Golston et al. (2020) and Section 3.2). However, a close comparison to the work of Golston et al. (2020) indicates that we observed higher NH_3 EmR during the afternoon peak in NH_3 emissions. Our average values are also higher than those reported by Eilerman et al. (2016) for summer only and for cattle specifically. (b) Before the sampling by Golston et al. (2020), estimates of NH_3 EmR in this region were limited to a handful of facilities. Our data set represents a dramatic increase in the number of facilities that can be used to estimate NH_3 EmR. While each prior study cited in Table 2 indicates a substantial step forward in terms of its technical and/or methodological approach, more observations are likely still needed to account for the true variability in NH_3 EmR, particularly outside of the warm summer months.

3.2. Temperature Dependencies

In general, Figure 3 shows that the highest NH_3 EmR observed during Phase One of TRANS^{2}Am were associated with the highest temperatures. Figure 4 explores the relationship between NH_3 EmR and temperature further.

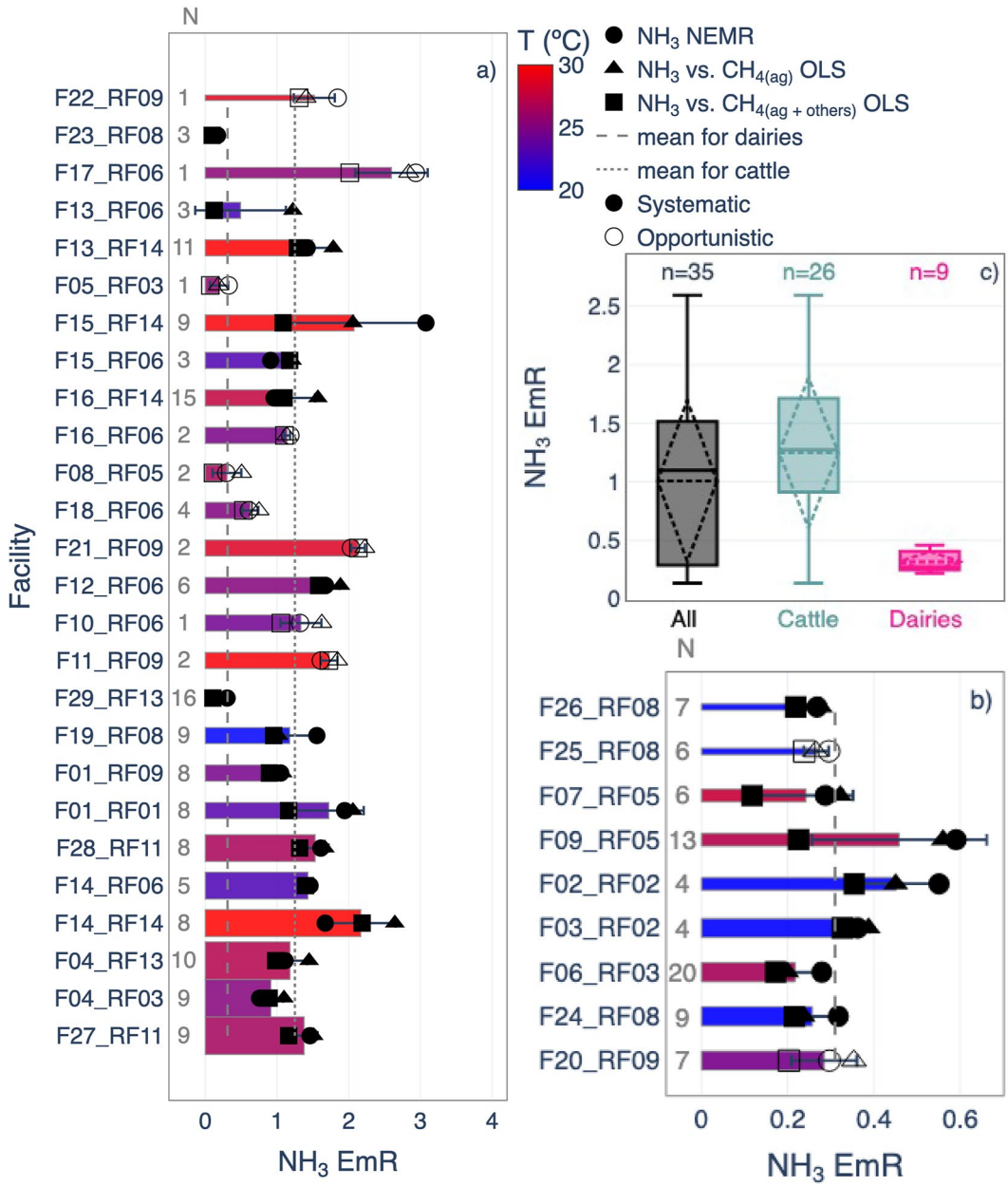

Figure 3. Average NH_3 emission ratios with respect to CH_4 (NH_3 EmR) for (a) beef cattle and (b) dairy facilities. NH_3 EmRs are calculated using all transects <10 km from the targeted facility. The number of transects used is shown in gray to the left of the colored bars. Bars are colored by the average ambient air temperature (°C) measured from the aircraft during the time of sampling, and bar width represents the maximum animal capacity reported (CDPHE, 2017). Bars with the smallest width represent those facilities for which there is no available information about animal capacity ($N = 3$; see Table 1 for more details). The different symbols represent different methods for estimating the NH_3 EmR. Circles indicate values calculated using the NH_3 NEMR method described in Section 2.5.2. Squares represent values calculated using in-plume observations and the OLS regression method as described in Section 2.5.2 (NH_3 vs. $CH_{4(ag + others)}$ OLS); triangles indicate values calculated using the OLS regression method with the multiple-predictors linear regression method for isolating CH_4 emissions associated with agricultural sources (Sections 2.5.3 and 2.5.4) (NH_3 vs. $CH_{4(ag)}$ OLS). Error bars show the standard deviation between the three methodologies. Filled and open symbols show estimates for facilities sampled systematically and opportunistically, respectively. Note that those facilities sampled opportunistically (open symbols) do not follow the sampling strategy (i.e., spiral + boxes downwind) outlined in Section 2.4.1 and usually include only a few transects (1–4). The dotted and dashed lines in Figures 2a and 2b represent the average NH_3 EmR for beef and dairy cattle, respectively, during Phase One of TRANS^{2}Am. (c) Average NH_3 EmR estimates for all facilities (black), separated by beef (blue) and dairy (pink).

Table 2
Comparison of Molar Emission Ratios and Emission Rates in the Colorado Front Range From Previous Publications

Study	Mean NH_3 EmR (error where reported) (ppbv ppbv^{-1})	Mean emission rate ($gNH_3 \cdot h^{-1} \cdot hd^{-1}$)	Number of facilities
Cattle			
This study	**1.2 (range = 0.1–2.6)**	**4–29**	**20/4**
Eilerman et al. (2016)	0.23 (+0.20/−0.11)		1
Golston et al. (2020)	0.25 (±0.03)	2.27 ± 0.23	15
Kille et al. (2017)		12 ± 2.8	1
Shonkwiler and Ham (2018)		3.33 ± 1.63	1
Sun et al. (2015)		2.64 ± 0.26	2
Pollack, McCabe, et al. (2022)	0.8–2.7	–	4
Dairy			
This study	**0.3 (range = 0.2–0.5)**	–	**9**
Eilerman et al. (2016)	0.14 (+0.13/−0.07) 0.17 (+0.08/−0.05)	–	2
Golston et al. (2020)	0.14 (±0.02)	5.33 ± 0.49	25
Kille et al. (2017)		11.4 ± 3.5	3

Note. Bold values denote highlight the values of this study.

Figure 4 shows the NH_3 EmR estimates as a function of temperature (°C) and relative humidity (%) for beef cattle (top panel) and dairy cows (lower panels). Panels (a) (cattle) and (c) (dairy) show the range of temperature and relative humidity of the data presented here, colored by NH_3 EmR and sized by facility maximum capacity. Panels (b) (cattle) and (d) (dairy) show NH_3 EmR versus temperature colored by relative humidity.

NH_3 EmR for beef cattle generally increases with increasing temperatures, consistent with prior work documenting an exponential relationship between NH_3 EmR and temperature for livestock facilities (Eilerman et al., 2016; Golston et al., 2020). In general, we observe a weak overall relationship between NH_3 EmR estimates and temperature for facilities housing beef cattle. The relationship between NH_3 EmR and temperature is especially hard to assess for the few NH_3 EmR estimates for dairies (panel d). Note that TRANS^{2}Am collected data in a small range of temperatures compared to those observed year-round in Colorado (Figure 4 panels a and c). Most of the data were collected during hot and dry conditions, and few observations were collected during hot and humid conditions, usually after precipitation events. Broadly consistent with our findings, the data presented by Golston et al. (2020) that were collected at temperatures >∼25°C also shows a large spread in NH_3 EmR ranging from near 0 up to almost 2 ppbv ppbv^{-1}. In both data sets, variability in NH_3 EmR appears larger in this uppermost temperature range.

The observed relationship between NH_3 EmR and temperature for beef cattle facilities is shown with the dashed line in panel (b). The temperature dependence of NH_3 emissions was derived using the principle that volatilization of NH_3 increases with higher temperature (Eilerman et al., 2016; Sander, 1999; Sutton et al., 1994). Briefly, the NH_3 compensation point for volatilization varies as a function of temperature and pH of the solution, both unknown for this data set. Here, we have used atmospheric temperatures as a proxy for soil temperature and coefficients that remain mostly constant with temperature and pH, allowing for a semi-empirical fit of the observations to the model (see Equations S1 and S2 in Supporting Information S1 for more details). Panel (b) shows that one of the highest estimates NH_3 EmR corresponds to the highest temperatures and lowest relative humidity in the range of observations (i.e., 2.2 ppbv ppbv^{-1}, 31°C, 21%). However, we observed a larger NH_3 EmR (i.e., ∼2.6 ppbv ppbv^{-1}) from an opportunistic sample at a lower temperature and higher relative humidity (i.e., 25°C, 27%). Pollack, McCabe, et al. (2022), McCabe et al. (2023) report NH_3 EmR estimates during November 2019 under colder conditions (median of 15°C) for five beef cattle facilities in the same study region. Their estimates range from 0.8 to 2.7 ppbv ppbv^{-1}. Similar to what Eilerman et al. (2016) observed, this suggests that large NH_3 EmR exist under colder conditions.

The few samples associated with lower temperatures (purple bars in Figure 3), higher relative humidities, and lower NH_3 EmR (i.e., facilities sampled during RF02 and RF08) were collected after regional precipitation events. Overall, most of the reduced nitrogen ($NH_x = NH_3 + NH_4^+$) in the near-source sampling is found in the gas phase as NH_3 (see Figure S10 in Supporting Information S1). Figure S10 in Supporting Information S1 shows

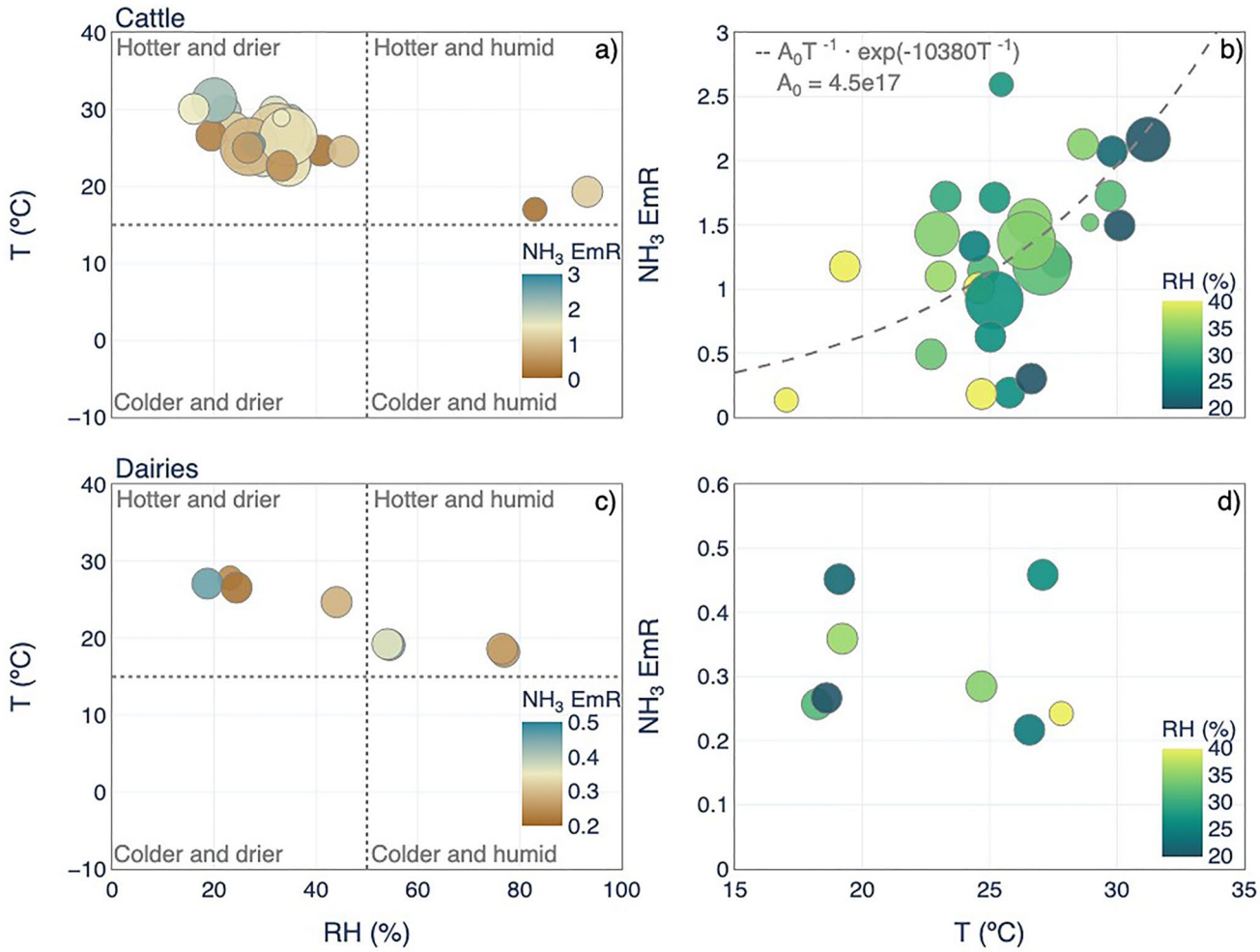

Figure 4. NH_3 EmRs (ppbv $ppbv^{-1}$) estimates for individual facilities as a function of temperature and relative humidity for beef cattle (top panels) and dairy cows (lower panels).

that the partitioning of NH_3 to the particle phase as NH_4^+ is, on average, less than 15% of the total NH_x for the data presented in this study. The few exceptions (RF02, RF03, and RF08) are those sampled after precipitation events, which, in general, have lower NH_3 mixing ratios (see Figure S11 in Supporting Information S1). To further explore the relationship between NH_3 emissions and temperature and based on previous observations that found a strong correlation between NH_3 emissions and time of the day (Eilerman et al., 2016), Figure 5 shows transect-specific NH_3 NERM (see Section 2.5.2) as a function of sampling time.

Figure 5 shows a diurnal pattern of NH_3 NEMR with higher values in the mid-afternoon and lower values in the morning and evening periods. The highest NEMRs were observed between 12 and 4 p.m. More quantitative information can be drawn from Figure 5 by examining some of the specific flights where that same facility was repeatedly sampled at different times and temperatures. F13, F14, F15, and F16 were sampled during both RF06 (pink dots in Figure 5) and RF14 (dark purple dots in Figure 5). RF06 was a mid-morning flight (10 a.m. to 1 p.m.) with average plume interception temperatures and relative humidities of ~23°C and 34%. RF14 was an afternoon flight (1–4 p.m.) with average plume interception temperatures and relative humidities of ~30°C and 21%. The NH_3 EmR estimates for these four facilities are 0.14–1.06 ppbv $ppbv^{-1}$ higher for RF14 (hotter and drier) than they are for RF06 (colder and more humid). F04, one of the biggest facilities sampled during Phase One of TRANS^{2}Am (see Figure 6 for details), was sampled during RF03 (light green dots in Figure 5) and RF13 (light purple dots in Figure 5). RF13 was a mid-morning flight (10 a.m. to 2 p.m.) with higher average temperature and relative humidity than RF03 (27°C vs. 25°C and 31% vs. 27%), a late afternoon flight (4–6 p.m.). The NH_3 EmR were higher during RF13 (hotter and more humid) than RF03 by 0.27 ppbv $ppbv^{-1}$ (Figure 7).

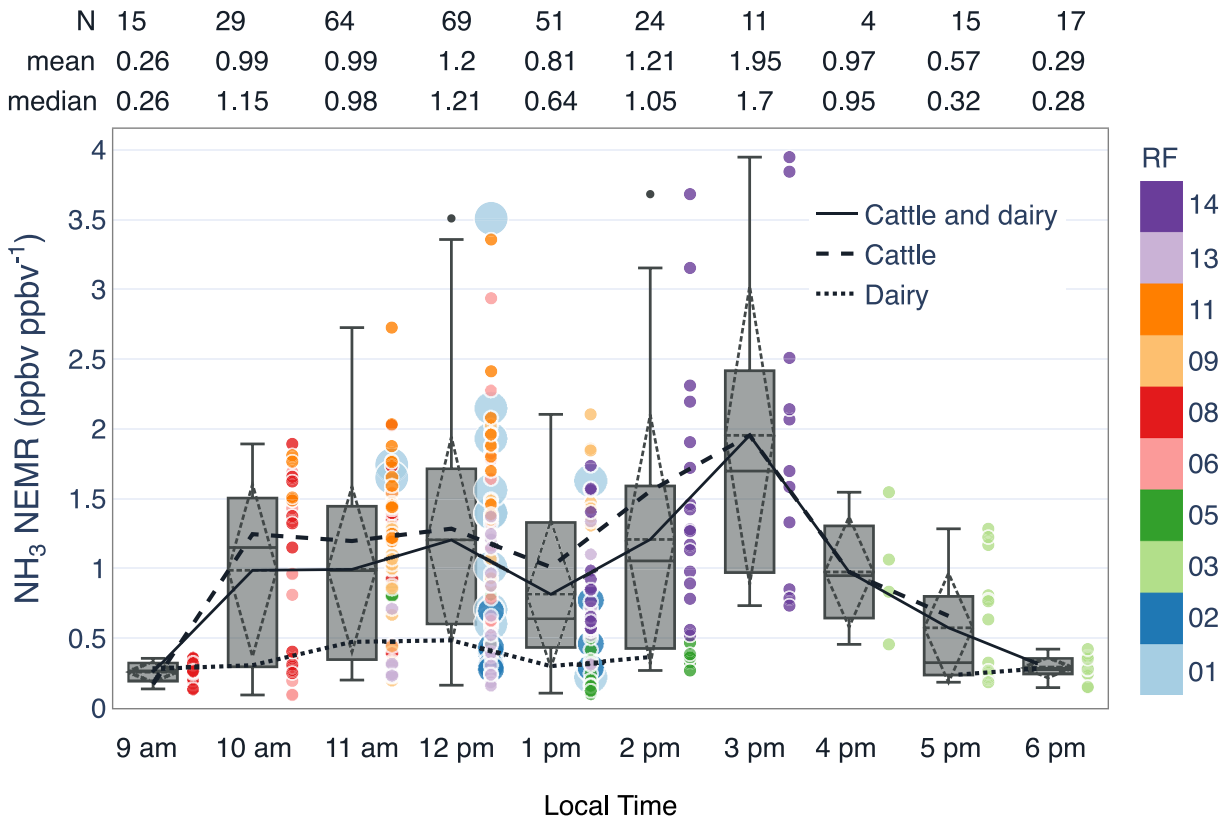

Figure 5. Transect-specific NH_3 NEMR as a function of local sampling time. The points represented by the boxplots are colored by research flight (RF). Points for RF01 (light blue) and RF02 (dark blue) were made larger intentionally to prevent masking from other data points. The lower and upper ends of the boxes span from quartile 1 (Q1) to quartile 3 (Q3). The whiskers correspond to each box edge (Q1 or Q3) ±1.5 the interquartile range (IQR: Q3–Q1). If no outliers are present, the whiskers represent minimum and maximum values. The dashed rhombuses show the sample mean (middle line) and the standard deviation (corners). *N* indicates the number of transects in each box plot. Note that all transects, including those >10 km and all animal types, have been included.

We also observed one case where higher temperatures did not produce a higher NEMR for a given facility. F01 was sampled twice (RF01 [light blue dots in Figure 5] and RF09 [light orange dots in Figure 5]) at roughly the same time of the day; the average temperature was slightly higher during RF09 (24.5°C) than during RF01 (23.2°C). However, the relative humidity was considerably higher during RF09 (45%) than during RF01 (30%). Despite a similar time of day and temperature range, NH_3 EmR estimates are lower for RF09 than they are for RF01 (1.00 vs. 1.972 ppbv $ppbv^{-1}$), suggesting that drier conditions favor NH_3 volatilization and emissions. The NH_3 emissions estimated for all these facilities and their differences in the context of different temperatures, relative humidities, and sampling times reflect the variability of NH_3 emissions for the same facility and their dependency on temperature, relative humidity, and time of day.

3.3. Plume Evolution Case Study

Loss of gas-phase NH_3 in plumes advected from feedlots can occur from dry deposition or chemical transformation of NH_3 to particle NH_4^+. Under the assumption of constant emissions relative to CH_4 and pseudo-Lagrangian sampling, we can use the ratio of NH_3 to CH_4 downwind of the CAFOs to constrain the loss of gas-phase NH_3, since both NH_3 and CH_4 are diluted similarly downwind of a source, but CH_4 does not undergo significant chemical losses in the temporal scales of this study (i.e., hours). Changes in the ratio of NH_3 to CH_4 downwind of the CAFOs can be used to calculate the total loss of NH_3 due to deposition or partitioning to the gas-phase (Lassman et al., 2020).

Across the data set presented in this work, we identified only one instance with substantial decay of NH_3 beyond 10 km from the facility: F04 during RF13. Note that the plume downwind of this facility did not decay similarly on the other sampling day (i.e., RF03). F04 was sampled on 23 August 2021, between 12:30 and 2 p.m. LT. F04 is one of the largest facilities housing beef cattle sampled during TRANS^{2}Am, with a reported animal maximum capacity of 100,000 animals. The plume intercepted from F04 during the RF13 shows the largest NH_3 mixing ratios observed

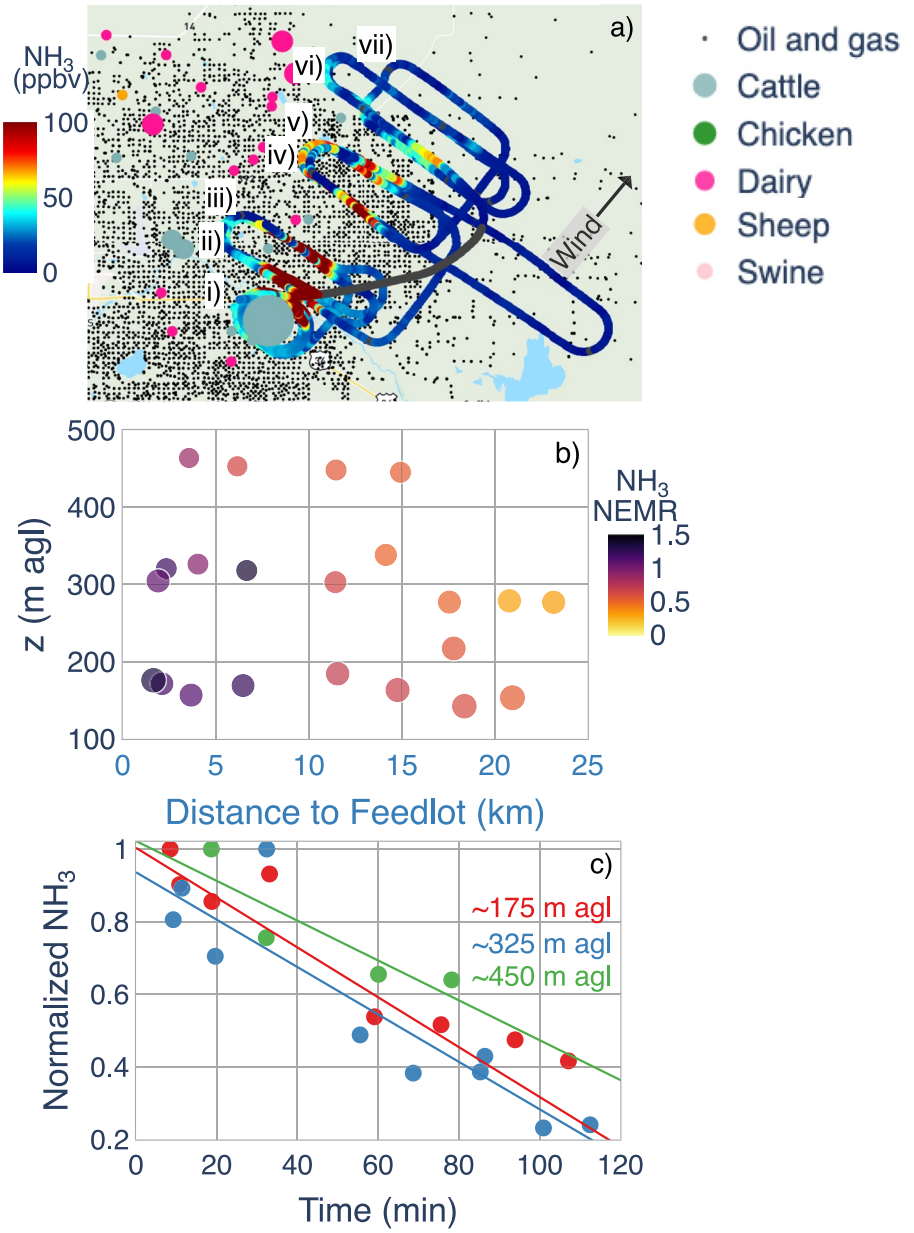

Figure 6. (a) Flight track of the UWKA colored by NH_3 (ppbv) during sampling of F04 on 23 August 2021. As in Figure 1, the colored and sized dots represent agricultural facilities housing different animals, and the black dots signify oil and gas operations as of 2015. Letters (i–vii) refer to different vertical transects used for emission rate calculations (refer to Figure S16 in Supporting Information S1 and Section 2.5.5 for more information). (b) Transect-specific NH_3 NEMR as a function of altitude above ground level (m agl) and distance downwind from the center of the facility (km). (c) Normalized NH_3 NEMR with respect to the maximum value in each altitude bin (~175, 325, and 450 m agl) as a function of the traveled time since emission (in minutes). Traveled time is calculated as the distance of each transect from the targeted facility divided by the average wind speed for that transect. Lines signify the linear fit for each altitude bin. E-folding time (time at which normalized NH_3 NEMR drops below $1/e$) was determined by the linear fit.

throughout Phase One of TRANS^{2}Am with values up to 440 ppbv of NH_3. The plume from F04 was intercepted up to 25 km downwind (Figure 6). The sampling included circles around the facility (as close as 2 km) and three distinct vertically stacked boxes at 4–6 km downwind, 11–14 km downwind, and 17–23 km downwind. The first two stacked boxes were executed at ~175, 325, and 450 m agl. The last one was executed only at 175 and 325 m agl. The PBL on this day contained two inversions. The lowest inversion was identified at ~500 m agl, and a second one was located at ~1,300 m agl (see Figure S12 in Supporting Information S1 for vertical profiles). Above the latter

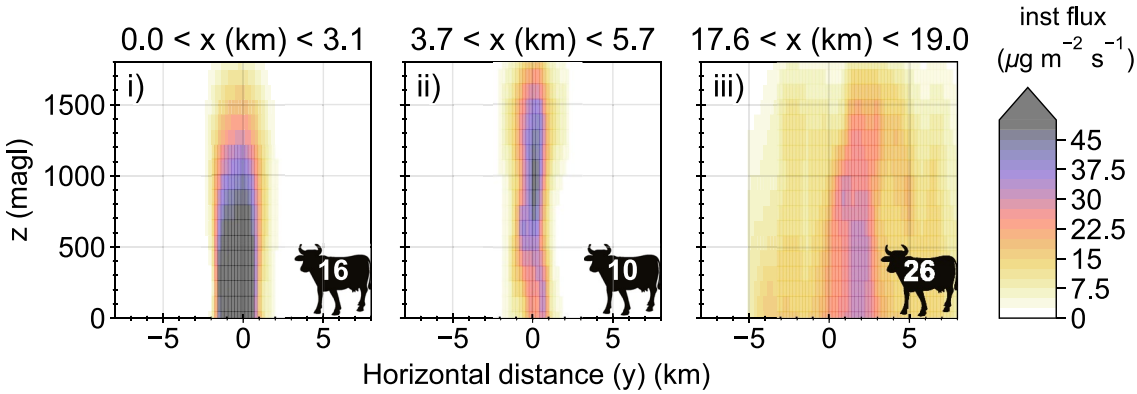

Figure 7. Example NH_3 emissions rates determined for F01 sampled during RF01 via transects at downwind distances of (a) 0–3.1 km, (b) 3.7–5.7 km, and (c) 17.6 and 19 km. The color bar shows inferred instantaneous horizontal fluxes in each grid cell in μg NH_3 m^{-2} s^{-1}. Grid cells are 200 (horizontal) × 100 (altitude) m. The number in the lower right corner shows the total inferred emission rates in g $NH_3 \cdot h^{-1} \cdot hd^{-1}$. Panels show simple linear interpolation using the python package *scipy.interpolate*, with a smooth factor of 1.

inversion, the BL appeared to be well-mixed. The maximum altitude that the aircraft reached was ~2,800 m agl, and thus characterization of the boundary layer above this altitude was not possible. In general, NH_3 NEMR decreased with distance from the facility after 10 km. The closest transects to the facility (175 and 325 m agl) have an average NH_3 NEMR of 1.11 (±0.19 std). The furthest transects (175 and 325 m agl) have an average NH_3 NEMR of 0.301 (±0.06). The calculated *e*-folding time for NH_3 NEMR at 175, 325, and 450 m agl are 108, 87, and 119.3 min, respectively. These estimates are not likely independent due to PBL mixing within the lower boundary layer.

3.4. NH_3 Emission Rates

Figure 7 shows inferred NH_3 emission rates for F01 during RF01, sampled from three distances downwind. The inferred emission rate magnitudes vary from 10 to 26 g $NH_3 \cdot h^{-1} \cdot hd^{-1}$ depending on where the calculation is performed. NH_3 inferred emission rates for F01, F04, F19, and F27/F28 range from 4 to 29 g $NH_3 \cdot h^{-1} \cdot hd^{-1}$. The average (std) is 14.4 (6.62) g $NH_3 \cdot h^{-1} \cdot hd^{-1}$. All these facilities house beef cattle. Similar to the example shown in Figure 7 (F01), the estimated NH_3 emission rates for F04, F19, and F27/28 depending on where the calculation is performed downwind from each facility. In general, there is no consistent relationship between the NH_3 emission rate and distance downwind (see Figure S13 in Supporting Information S1). For more details, refer to Table 1 and Figures S14–S16 in Supporting Information S1. The emission rates for F27 and F28 are combined estimates since these facilities are within ~8 km of each other, and their plumes merged during sampling. Note that the NH_3 emission rates estimates for F04 during RF13 are presented for curtains >10 km from F04, where substantial NH_3 loss was observed (see Figure 6). If the curtains >10 km are not included, the average NH_3 emission rate for F04 during RF13 increases from 11.8 to 17 g $NH_3 \cdot h^{-1} \cdot hd^{-1}$ which is closer to the estimates of the other two larger facilities (F01 and F27/28). Unlike NH_3 emissions ratios, inferred NH_3 emission rates do not require correction for CH_4 emissions.

The average of our estimates is higher than those reported in previous studies (i.e., 2.64–12 g $NH_3 \cdot hd^{-1} \cdot h^{-1}$ Golston et al., 2020; Kille et al., 2017; Shonkwiler & Ham, 2018; Sun et al., 2015) with one exception that reports NH_3 emission rates 14 (±2) g $NH_3 \cdot hd^{-1} \cdot h^{-1}$ for one facility (F04 in this study) (McCabe et al., 2023). Differences between our findings and previous results could be explained by (a) a single sample per facility, (b) the different methodology sample NH_3 (i.e., airborne observations vs. ground observations), or they may more fully reflect the variability in emissions in space and time. Our estimates are also larger than those reported from other regions. For example, emission rates measured for facilities in Alberta, Canada, report values of 5.83 and 8.5 g $NH_3 \cdot h^{-1} \cdot hd^{-1}$, which are in the lower range of what we observed in northeastern Colorado (McGinn et al., 2007; Staebler et al., 2009). Shonkwiler and Ham (2018) summarize other studies of NH_3 emission rates in other places in the United States and worldwide during different seasons. NH_3 emissions rates estimates of 2.6 and 5.75–8 g $\cdot h^{-1} \cdot hd^{-1}$ have been observed downwind of small feedlots (<1,200 beef cattle) in China (Yang et al., 2016) and Australia (Denmead et al., 2008), respectively.

4. Conclusions

Here, we report on summertime airborne observations of NH_3 and CH_4 collected over northeastern Colorado during the first phase of the TRANS^{2}Am field intensive. We intercepted plumes downwind of 29 dairies and

cattle feedlots, and we used these observations to infer NH_3 emissions ratios (EmR) with respect to CH_4 and NH_3 horizontal emission rates for a subset of facilities. We show the following:

- NH_3 EmR during August 2021 ranged from 0.1 to 2.6 ppbv ppbv^{-1}, which are larger than those presented in previous literature. The NH_3 EmR associated with beef cattle feedlots are, on average, four times larger than NH_3 EmR associated with dairies (1.2 vs. 0.3 ppbv ppbv^{-1}, respectively).
- The study region presents a complex combination of emissions sources, especially for CH_4, which has substantial emissions from both oil and gas operations and agriculture intermixed. We present four estimates of NH_3 EmR with and without correction for CH_4 emissions from oil and gas operations. Estimates that account for intermixed oil and gas CH_4 emissions (NH_3 NEMR and OLS regression with agriculturally specific CH_4) are higher than NH_3 EmR based on methods that do not account for intermixed oil and gas CH_4 emissions (OLS regression with uncorrected CH_4). Accounting for CH_4 emissions from oil and gas operations is likely more important for aircraft observations than ground-based observations that sample immediately adjacent to facilities. However, prior work that has not accounted for other emissions sources may underestimate NH_3 EmR in the region.
- In the region immediately downwind of the diaries and cattle feedlots we sampled, particle phase NH_4^+ accounted for <15% of the absolute NH_x on average.
- Prior work has reported correlations between NH_3 EmR and temperature. However, data from Phase One of TRANS^{2}Am represent a relatively small temperature range. Even though we document a general trend of increasing NH_3 EmR with temperature, we also observed high NH_3 EmR at lower temperatures with high relative humidities.
- NH_3 NEMRs have a relationship with time of day, with higher NH_3 NEMRs between 12 and 4 p.m. LT. For five of the six facilities sampled on different days, NH_3 NEMRs are higher for samples collected under hotter and drier conditions as well as later in the day.
- We document NH_3 decay relative to CH_4 within the plume associated with the largest facility (F04) sampled during Phase One of TRANS^{2}Am. This plume contained the highest NH_3 mixing ratios observed during the campaign. The plume encountered downwind of F04 during RF13 had an e-folding time of 108, 87, and 119.3 min for samples collected downwind at 175, 325, and 450 m agl. While the decay was clear on RF13, the plume downwind of F04 did not show similar decay during its sampling on RF03.
- Our inferred horizontal emissions rate estimates for NH_3 for four beef cattle facilities range from 4 to 29 g $NH_3 \cdot h^{-1} \cdot hd^{-1}$ with an average (std) of 14.4 (6.62) g $NH_3 \cdot h^{-1} \cdot hd^{-1}$. We observe larger NH_3 emission rates (g $NH_3 \cdot h^{-1} \cdot hd^{-1}$) compared to other studies, with one exception. We do not find a relationship between maximum reported animal capacity and inferred horizontal NH_3 emissions rates.

Phase One of TRANS^{2}Am substantially increases the number of in situ measurements of NH_3 emissions and their relationship with CH_4 from facilities housing beef cattle and dairy cows in northeastern Colorado. These data represent the warmest part of the seasonal cycle. Future work should focus on colder, more humid conditions characteristic of other times of the year. These data show the variability associated with NH_3 emissions from CAFOs during hot and dry conditions. Forthcoming papers will discuss similar data collected during the second phase of the campaign conducted in August 2022 and data from research flights focused on the evolution of large regional plumes as they move from the polluted Front Range up into the Rocky Mountains.

Conflict of Interest

The authors declare no conflicts of interest relevant to this study.

Data Availability Statement

In situ, ammonia (Pollack, Juncosa Calahorrano, & Fischer, 2022), nitric acid (Pollack, Juncosa Calahorrano, et al., 2022), methane (Caulton & McCabe, 2022a; Caulton & Steinmann, 2023a), ethane (Caulton & McCabe, 2022b; Caulton & Steinmann, 2023b), Particle Into Liquid Sampler (Sullivan & Fischer, 2023), and the University of Wyoming King Air (UWKA) meteorological data (French et al., 2023) collected during Phase One of TRANS^{2}Am was used for this research. Colorado livestock information was accessed through the database maintained by the Colorado Department of Public Health and Environment (CDPHE, 2017). All the analysis was done using Python V3.7.6. Figures presented in this manuscript were done using Plotly (Plotly Technologies Inc., 2015) and ProPlot (Davis, 2021).

Acknowledgments
The funding for this work was provided by the US National Science Foundation (NSF award number AGS-2020127). The authors wish to thank the University of Wyoming King Air team for their many contributions to supporting the field deployment. The authors would like to thank Allie Mazurek and Marqi Rocque for their forecasting support during Phase One of TRANS^{2}Am.

References

Bauer, S. E., Tsigaridis, K., & Miller, R. (2016). Significant atmospheric aerosol pollution caused by world food cultivation. *Geophysical Research Letters*, *43*(10), 5394–5400. https://doi.org/10.1002/2016GL068354

Benedict, K. B., Carrico, C. M., Kreidenweis, S. M., Schichtel, B., Malm, W. C., & Collett, J. L. (2013a). A seasonal nitrogen deposition budget for Rocky Mountain National Park. *Ecological Applications*, *23*(5), 1156–1169. https://doi.org/10.1890/12-1624.1

Benedict, K. B., Day, D., Schwandner, F. M., Kreidenweis, S. M., Schichtel, B., Malm, W. C., & Collett, J. L. (2013b). Observations of atmospheric reactive nitrogen species in Rocky Mountain National Park and across northern Colorado. *Atmospheric Environment*, *64*, 66–76. https://doi.org/10.1016/j.atmosenv.2012.08.066

Bobbink, R., Hicks, K., Galloway, J., Spranger, T., Alkemade, R., Ashmore, M., et al. (2010). Global assessment of nitrogen deposition effects on terrestrial plant diversity: A synthesis. *Ecological Applications*, *20*(1), 30–59. https://doi.org/10.1890/08-1140.1

Cady-Pereira, K. E., Guo, X., Wang, R., Leytem, A., Calkins, C., Berry, E., et al. (2023). Validation of NH 3 observations from AIRS and CrIS against aircraft measurements from DISCOVER-AQ and a surface network in the Magic Valley [Preprint]. Gases/Remote Sensing/Validation and Intercomparisons. https://doi.org/10.5194/amt-2022-336

Caulton, D., & McCabe, M. (2022a). TRANS2AM: King Air Picarro G2401-M 2021 Phase Data. Version 2.0 [Dataset]. UCAR/NCAR – Earth Observing Laboratory. https://doi.org/10.26023/8EMT-47X7-VV00

Caulton, D., & McCabe, M. (2022b). TRANS2AM: King Air QC-TILDAS Gas Phase C2H6 2021 Phase Data. Version 1.0 [Dataset]. UCAR/NCAR – Earth Observing Laboratory. https://doi.org/10.26023/90F8-011X-RE10

Caulton, D., & Steinmann, K. (2023a). TRANS2AM: King Air Picarro G2401-M 2022 Phase Data. Version 1.0. UCAR/NCAR - Earth Observing Laboratory. https://doi.org/10.26023/WCS6-S5BC-EF0T

Caulton, D., & Steinmann, K. (2023b). TRANS2AM: King Air QC-TILDAS Gas Phase C2H6 2022 Phase Data. Version 1.0. UCAR/NCAR - Earth Observing Laboratory. https://doi.org/10.26023/5Y1S-N2GB-C505

Cazorla, M., & Juncosa, J. (2018). Planetary boundary layer evolution over an equatorial Andean valley: A simplified model based on balloon-borne and surface measurements. *Atmospheric Science Letters*, *19*(8), e829. https://doi.org/10.1002/asl.829

CDPHE (2017). Animal and livestock feeding operations. Retrieved from www.colorado.gov/pacific/cdphe/animal-and-livestock-feeding-operations

Clarisse, L., Clerbaux, C., Dentener, F., Hurtmans, D., & Coheur, P.-F. (2009). Global ammonia distribution derived from infrared satellite observations. *Nature Geoscience*, *2*(7), 479–483. https://doi.org/10.1038/ngeo551

Crosson, E. R. (2008). A cavity ring-down analyzer for measuring atmospheric levels of methane, carbon dioxide, and water vapor. *Applied Physics B*, *92*(3), 403–408. https://doi.org/10.1007/s00340-008-3135-y

Davidson, E. A., David, M. B., Galloway, J. N., Goodale, C. L., Haeuber, R., Harrison, J. A., et al. (2011). Excess nitrogen in the U.S. environment: Trends, risks, and solutions. *Issues in Ecology, 15. USGS Publications Warehouse*. Retrieved from https://pubs.usgs.gov/publication/70032270

Davis, L. L. B. (2021). ProPlot [Software]. *Zenodo*. https://doi.org/10.5281/zenodo.3873878

Denmead, O. T., Chen, D., Griffith, D. W. T., Loh, Z. M., Bai, M., & Naylor, T. (2008). Emissions of the indirect greenhouse gases NH_3 and NOx from Australian beef cattle feedlots. *Australian Journal of Experimental Agriculture*, *48*(2), 213. https://doi.org/10.1071/EA07276

Eilerman, S. J., Peischl, J., Neuman, J. A., Ryerson, T. B., Aikin, K. C., Holloway, M. W., et al. (2016). Characterization of ammonia, methane, and nitrous oxide emissions from concentrated animal feeding operations in northeastern Colorado. *Environmental Science & Technology*, *50*(20), 10885–10893. https://doi.org/10.1021/acs.est.6b02851

Ellis, R. A., Murphy, J. G., Pattey, E., van Haarlem, R., O'Brien, J. M., & Herndon, S. C. (2010). Characterizing a Quantum Cascade Tunable Infrared Laser Differential Absorption Spectrometer (QC-TILDAS) for measurements of atmospheric ammonia. *Atmospheric Measurement Techniques*, *3*(2), 397–406. https://doi.org/10.5194/amt-3-397-2010

Environmental Protection Agency (EPA), The National Emission Inventory (NEI) (2017). Retrieved from https://www.epa.gov/air-emissions-inventories/2017-national-emissions-inventory-nei-data

French, J., Oolman, L., & Plummer, D. (2023). University of Wyoming King Air (UWKA) High-Rate Flight Level Data for TRANS2AM 2021 Phase Version 1.0 [Dataset]. UCAR/NCAR - Earth Observing Laboratory. https://doi.org/10.26023/TKV3-WJ7T-PP0J

Golston, L. M., Pan, D., Sun, K., Tao, L., Zondlo, M. A., Eilerman, S. J., et al. (2020). Variability of ammonia and methane emissions from animal feeding operations in northeastern Colorado. *Environmental Science & Technology*, *54*(18), 11015–11024. https://doi.org/10.1021/acs.est.0c00301

Hacker, J. M., Chen, D., Bai, M., Ewenz, C., Junkermann, W., Lieff, W., et al. (2016). Using airborne technology to quantify and apportion emissions of CH_4 and NH_3 from feedlots. *Animal Production Science*, *56*(3), 190. https://doi.org/10.1071/AN15513

Heald, C. L., Collett, J. L., Lee, T., Benedict, K. B., Schwandner, F. M., Li, Y., et al. (2012). Atmospheric ammonia and particulate inorganic nitrogen over the United States. *Atmospheric Chemistry and Physics*, *12*(21), 10295–10312. https://doi.org/10.5194/acp-12-10295-2012

Holmes, C. D. (2018). Methane feedback on atmospheric chemistry: Methods, models, and mechanisms. *Journal of Advances in Modeling Earth Systems*, *10*(4), 1087–1099. https://doi.org/10.1002/2017MS001196

Huntington, G. B., & Archibeque, S. L. (2000). Practical aspects of urea and ammonia metabolism in ruminants. *Journal of Animal Science*, *77*(E-Suppl), 1. https://doi.org/10.2527/jas2000.77E-Suppl1y

IPCC. (2021). In P. Zhai, A. Pirani, S. L. Connors, C. Péan, et al. (Eds.), *Climate change 2021: The physical science basis. Contribution of working group I to the sixth assessment report of the intergovernmental panel on climate change[Masson-Delmotte*. Cambridge University Press. In Press. https://doi.org/10.1017/9781009157896

Karydis, V. A., Tsimpidi, A. P., Pozzer, A., & Lelieveld, J. (2021). How alkaline compounds control atmospheric aerosol particle acidity. *Atmospheric Chemistry and Physics*, *21*(19), 14983–15001. https://doi.org/10.5194/acp-21-14983-2021

Kille, N., Baidar, S., Handley, P., Ortega, I., Sinreich, R., Cooper, O. R., et al. (2017). The CU mobile Solar Occultation Flux instrument: Structure functions and emission rates of NH_3, NO_2 and C_2H_6. *Atmospheric Measurement Techniques*, *10*(1), 373–392. https://doi.org/10.5194/amt-10-373-2017

Kille, N., Chiu, R., Frey, M., Hase, F., Sha, M. K., Blumenstock, T., et al. (2019). Separation of methane emissions from agricultural and natural gas sources in the Colorado Front Range. *Geophysical Research Letters*, *46*(7), 3990–3998. https://doi.org/10.1029/2019GL082132

Kim, S.-W., Heckel, A., McKeen, S. A., Frost, G. J., Hsie, E.-Y., Trainer, M. K., et al. (2006). Satellite-observed U.S. power plant NO_x emission reductions and their impact on air quality. *Geophysical Research Letters*, *33*(22), L22812. https://doi.org/10.1029/2006GL027749

Lassman, W., Collett, J. L., Ham, J. M., Yalin, A. P., Shonkwiler, K. B., & Pierce, J. R. (2020). Exploring new methods of estimating deposition using atmospheric concentration measurements: A modeling case study of ammonia downwind of a feedlot. *Agricultural and Forest Meteorology*, *290*, 107989. https://doi.org/10.1016/j.agrformet.2020.107989

Li, Y., Schichtel, B. A., Walker, J. T., Schwede, D. B., Chen, X., Lehmann, C. M. B., et al. (2016). Increasing importance of deposition of reduced nitrogen in the United States. *Proceedings of the National Academy of Sciences of the United States of America*, *113*(21), 5874–5879. https://doi.org/10.1073/pnas.1525736113

Liu, L., Xu, W., Lu, X., Zhong, B., Guo, Y., Lu, X., et al. (2022). Exploring global changes in agricultural ammonia emissions and their contribution to nitrogen deposition since 1980. *Proceedings of the National Academy of Sciences of the United States of America*, *119*(14), e2121998119. https://doi.org/10.1073/pnas.2121998119

Marple, V. A., Rubow, K. L., & Behm, S. M. (1991). A Microorifice Uniform Deposit Impactor (MOUDI): Description, calibration, and use. *Aerosol Science and Technology*, *14*(4), 434–446. https://doi.org/10.1080/02786829108959504

McCabe, M. E., Pollack, I. B., Fischer, E. V., Steinmann, K. M., & Caulton, D. R. (2023). Technical note: Isolating methane emissions from animal feeding operations in an interfering location. *Atmospheric Chemistry and Physics*, *23*(13), 7479–7494. https://doi.org/10.5194/acp-23-7479-2023

McGinn, S. M., Flesch, T. K., Crenna, B. P., Beauchemin, K. A., & Coates, T. (2007). Quantifying ammonia emissions from a cattle feedlot using a dspersion model. *Journal of Environmental Quality*, *36*(6), 1585–1590. https://doi.org/10.2134/jeq2007.0167

McManus, J. B. (2010). Application of quantum cascade lasers to high-precision atmospheric trace gas measurements. *Optical Engineering*, *49*(11), 111124. https://doi.org/10.1117/1.3498782

McManus, J. B., Kebabian, P. L., & Zahniser, M. S. (1995). Astigmatic mirror multipass absorption cells for long-path-length spectroscopy. *Applied Optics*, *34*(18), 3336. https://doi.org/10.1364/AO.34.003336

Meng, W., Zhong, Q., Yun, X., Zhu, X., Huang, T., Shen, H., et al. (2017). Improvement of a global high-resolution ammonia emission inventory for combustion and industrial sources with new data from the residential and transportation sectors. *Environmental Science & Technology*, *51*(5), 2821–2829. https://doi.org/10.1021/acs.est.6b03694

Miller, D. J., Sun, K., Tao, L., Khan, M. A., & Zondlo, M. A. (2014). Open-path, quantum cascade-laser-based sensor for high-resolution atmospheric ammonia measurements. *Atmospheric Measurement Techniques*, *7*(1), 81–93. https://doi.org/10.5194/amt-7-81-2014

Ndegwa, P. M., Hristov, A. N., Arogo, J., & Sheffield, R. E. (2008). A review of ammonia emission mitigation techniques for concentrated animal feeding operations. *Biosystems Engineering*, *100*(4), 453–469. https://doi.org/10.1016/j.biosystemseng.2008.05.010

Neuman, J. A., Ryerson, T. B., Huey, L. G., Jakoubek, R., Nowak, J. B., Simons, C., & Fehsenfeld, F. C. (2003). Calibration and evaluation of nitric acid and ammonia permeation tubes by UV optical absorption. *Environmental Science & Technology*, *37*(13), 2975–2981. https://doi.org/10.1021/es0264221

Nowak, J. B., Neuman, J. A., Bahreini, R., Middlebrook, A. M., Holloway, J. S., McKeen, S. A., et al. (2012). Ammonia sources in the California South Coast Air Basin and their impact on ammonium nitrate formation. *Geophysical Research Letters*, *39*(7), n/a. https://doi.org/10.1029/2012GL051197

Orsini, D. A., Ma, Y., Sullivan, A., Sierau, B., Baumann, K., & Weber, R. J. (2003). Refinements to the particle-into-liquid sampler (PILS) for ground and airborne measurements of water soluble aerosol composition. *Atmospheric Environment*, *37*(9–10), 1243–1259. https://doi.org/10.1016/S1352-2310(02)01015-4

Pan, D., Benedict, K. B., Golston, L. M., Wang, R., Collett, J. L., Tao, L., et al. (2021). Ammonia dry deposition in an alpine ecosystem traced to agricultural emission hotpots. *Environmental Science & Technology*, *55*(12), 7776–7785. https://doi.org/10.1021/acs.est.0c05749

Plotly Technologies Inc. (2015). Collaborative data science [Software]. Plotly Technologies Inc. Retrieved from https://plot.ly

Pollack, I. B., Juncosa Calahorrano, J. F., & Fischer, E. V. (2022). TRANS2AM: King Air QC-TILDAS Gas Phase NH_3 2021 Phase Data Version 1.0 [Dataset]. UCAR/NCAR – Earth Observing Laboratory. https://doi.org/10.26023/F498-J3C0-ZS0R

Pollack, I. B., Juncosa Calahorrano, J. F., Roscioli, J. R., & Fischer, E. V. (2022). TRANS2AM: King Air QC-TILDAS Gas Phase HNO_3 2021 Phase Data Version 1.0 [Dataset]. UCAR/NCAR – Earth Observing Laboratory. https://doi.org/10.26023/C680-Z0QB-XY05

Pollack, I. B., Lindaas, J., Roscioli, J. R., Agnese, M., Permar, W., Hu, L., & Fischer, E. V. (2019). Evaluation of ambient ammonia measurements from a research aircraft using a closed-path QC-TILDAS operated with active continuous passivation. *Atmospheric Measurement Techniques*, *12*(7), 3717–3742. https://doi.org/10.5194/amt-12-3717-2019

Pollack, I. B., McCabe, M. E., Caulton, D. R., & Fischer, E. V. (2022). Enhancements in ammonia and methane from agricultural sources in the northeastern Colorado Front Range using observations from a small research aircraft. *Environmental Science & Technology*, *56*(4), 2236–2247. https://doi.org/10.1021/acs.est.1c07382

Preece, S. L. M., Cole, A. N., Todd, R. W., & Auvermann, B. W. (2017). *Ammonia emissions from cattle feeding operations*. Texas A&M AgriLife Extension Service, E-632, 12.

Roscioli, J. R., Zahniser, M. S., Nelson, D. D., Herndon, S. C., & Kolb, C. E. (2016). New approaches to measuring sticky molecules: Improvement of instrumental response times using active passivation. *The Journal of Physical Chemistry A*, *120*(9), 1347–1357. https://doi.org/10.1021/acs.jpca.5b04395

Sander, R. (1999). Modeling atmospheric chemistry: Interactions between gas-phase species and liquid cloud/aerosol particles. *Surveys in Geophysics*, *20*(1), 1–31. https://doi.org/10.1023/a:1006501706704

Shonkwiler, K. B., & Ham, J. M. (2018). Ammonia emissions from a beef feedlot: Comparison of inverse modeling techniques using long-path and point measurements of fenceline NH_3. *Agricultural and Forest Meteorology*, *258*, 29–42. https://doi.org/10.1016/j.agrformet.2017.10.031

Snider, J., Petters, M., Takagi, H., Liu, P., Lukens, D., Glover, B., et al. (2018). The NCAR-UWyo aerosol inlet. Retrieved from http://www-das.uwyo.edu/~jsnider/inlet_report_v02.pdf

Sorooshian, A., Brechtel, F. J., Ma, Y., Weber, R. J., Corless, A., Flagan, R. C., & Seinfeld, J. H. (2006). Modeling and characterization of a particle-into-liquid sampler (PILS). *Aerosol Science and Technology*, *40*(6), 396–409. https://doi.org/10.1080/02786820600632282

Staebler, R. M., McGinn, S. M., Crenna, B. P., Flesch, T. K., Hayden, K. L., & Li, S.-M. (2009). Three-dimensional characterization of the ammonia plume from a beef cattle feedlot. *Atmospheric Environment*, *43*(38), 6091–6099. https://doi.org/10.1016/j.atmosenv.2009.08.045

Sullivan, A., & Fischer, E. (2023). TRANS2AM: King air PILS water-soluble aerosol components data Version 2.0 [Dataset]. UCAR/NCAR – Earth Observing Laboratory. https://doi.org/10.26023/680R-9WEZ-N70H

Sullivan, A. P., Pokhrel, R. P., Shen, Y., Murphy, S. M., Toohey, D. W., Campos, T., et al. (2022). Examination of brown carbon absorption from wildfires in the western US during the WE-CAN study. *Atmospheric Chemistry and Physics*, *22*(20), 13389–13406. https://doi.org/10.5194/acp-22-13389-2022

Sun, K., Tao, L., Miller, D. J., Zondlo, M. A., Shonkwiler, K. B., Nash, C., & Ham, J. M. (2015). Open-path eddy covariance measurements of ammonia fluxes from a beef cattle feedlot. *Agricultural and Forest Meteorology*, *213*, 193–202. https://doi.org/10.1016/j.agrformet.2015.06.007

Sutton, M. A., Asman, W. A. H., & Schjørring, J. K. (1994). Dry deposition of reduced nitrogen. *Tellus B: Chemical and Physical Meteorology*, *46*(4), 255–273. https://doi.org/10.1034/j.1600-0889.1994.t01-2-00002.x

Tong, D. Q., Lamsal, L., Pan, L., Ding, C., Kim, H., Lee, P., et al. (2015). Long-term NOx trends over large cities in the United States during the great recession: Comparison of satellite retrievals, ground observations, and emission inventories. *Atmospheric Environment*, *107*, 70–84. https://doi.org/10.1016/j.atmosenv.2015.01.035

USDA. (2012). NASS. 2012 Census of Agriculture. Retrieved from http://www.nass.usda.gov/Publications/AgCensus/2012/

Van Damme, M., Clarisse, L., Whitburn, S., Hadji-Lazaro, J., Hurtmans, D., Clerbaux, C., & Coheur, P.-F. (2018). Industrial and agricultural ammonia point sources exposed. *Nature*, *564*(7734), 99–103. https://doi.org/10.1038/s41586-018-0747-1

Wyer, K. E., Kelleghan, D. B., Blanes-Vidal, V., Schauberger, G., & Curran, T. P. (2022). Ammonia emissions from agriculture and their contribution to fine particulate matter: A review of implications for human health. *Journal of Environmental Management*, *323*, 116285. https://doi.org/10.1016/j.jenvman.2022.116285

Xu, R., Tian, H., Pan, S., Prior, S. A., Feng, Y., Batchelor, W. D., et al. (2019). Global ammonia emissions from synthetic nitrogen fertilizer applications in agricultural systems: Empirical and process-based estimates and uncertainty. *Global Change Biology*, *25*(1), 314–326. https://doi.org/10.1111/gcb.14499

Yacovitch, T. I., Herndon, S. C., Roscioli, J. R., Floerchinger, C., McGovern, R. M., Agnese, M., et al. (2014). Demonstration of an ethane spectrometer for methane source identification. *Environmental Science & Technology*, *48*(14), 8028–8034. https://doi.org/10.1021/es501475q

Yang, Y., Liao, W., Wang, X., Liu, C., Xie, Q., Gao, Z., et al. (2016). Quantification of ammonia emissions from dairy and beef feedlots in the Jing-Jin-Ji district, China. *Agriculture, Ecosystems & Environment*, *232*, 29–37. https://doi.org/10.1016/j.agee.2016.07.016

Zahniser, M. S., Nelson, D. D., McManus, J. B., Kebabian, P. L., & Lloyd, D. (1995). Measurement of trace gas fluxes using tunable diode laser spectroscopy. *Philosophical Transactions of the Royal Society of London*, *351*(1696), 371–382. https://doi.org/10.1098/rsta.1995.0040

Zhan, X., Bo, Y., Zhou, F., Liu, X., Paerl, H. W., Shen, J., et al. (2017). Evidence for the importance of atmospheric nitrogen deposition to Eutrophic Lake Dianchi, China. *Environmental Science & Technology*, *51*(12), 6699–6708. https://doi.org/10.1021/acs.est.6b06135

Zhu, L., Henze, D. K., Bash, J. O., Cady-Pereira, K. E., Shephard, M. W., Luo, M., & Capps, S. L. (2015). Sources and impacts of atmospheric NH_3: Current understanding and frontiers for modeling, measurements, and remote sensing in North America. *Current Pollution Reports*, *1*(2), 95–116. https://doi.org/10.1007/s40726-015-0010-4